

A general analytical framework for the mechanics of heterogeneous hexagonal lattices

S. Mukherjee^{a,*}, S. Adhikari^a

^a*College of Engineering, Swansea University, Bay Campus, Fabian Way, Swansea SA1 8EN, UK*

Abstract

The in-plane mechanics of two-dimensional heterogeneous hexagonal lattices are investigated. The heterogeneity originates from two physically realistic considerations: different constituent materials and different wall thicknesses. Through the combination of multi-material and multi-thickness elements, the most general form of 2D heterogeneous hexagonal lattices is proposed in this paper. By exploiting the mechanics of a unit cell with multi-material and multi-thickness characteristics, exact closed-form analytical expressions of equivalent elastic properties of the general heterogeneous lattice have been derived. The equivalent elastic properties of the 2D heterogeneous lattice are Young's moduli and Poisson's ratios in both directions and the shear modulus. Two distinct cases, namely lattices with thin and thick constituent members, are considered. Euler-Bernoulli beam theory is employed for the thin-wall case, and Timoshenko beam theory is employed for the thick-wall case. The closed-form expressions are validated by independent finite element simulation results. The generalised expressions can be considered as benchmark solutions for validating future numerical and experimental investigations. The conventional single-material and single-thickness homogeneous lattice appears as a special case of the heterogeneous considered here. By introducing the Material Disparity Ratio (MDR) and Geometric Disparity Ratio (GDR), variability in the equivalent elastic properties has been graphically demonstrated. As opposed to classical homogeneous lattices, heterogeneous lattices significantly expand the design space for 2D lattices. Orders-of-magnitude of variability in the equivalent elastic properties is possible by suitably selecting material and geometric disparities within the lattices. The general closed-form expressions proposed in this paper open up the opportunity to design next-generation heterogeneous lattices with highly tailored effective elastic properties.

Keywords: Hexagonal lattices; stiffness matrix; homogeneous properties; elastic constants; 2D materials

1. Introduction

Mechanical metamaterials are formed by arranging different micro-structures to achieve the user defined novel macro-scale properties [1]. Lattice based mechanical metamaterials

*Corresponding author.

Email addresses: shuvajit.mukherjee@swansea.ac.uk (S. Mukherjee),
S.Adhikari@swansea.ac.uk (S. Adhikari)

are formed by arranging the periodic unit cell in some particular arrangement to obtain unprecedented effective material properties. The unit cell of a lattice is generally formed of a different basic structural element based on the application requirements. The microstructure of the unit cell and material properties of the constituent elements define the overall properties (such as equivalent elastic moduli, Poisson's ratios, buckling strength, energy absorption, vibration and wave propagation characteristics) of the lattice material. The work of Gibson and Ashby [2] and Fleck et. al. [3] can be referred to as understanding the concept of cellular materials. Due to the advancement of additive manufacturing we have the scope of exploiting innovative micro-structural design [4–6] to explore the fascinating material properties which are not possible in naturally occurring materials. Most of the work in literature deals with developing microarchitected lattice metamaterials with single material for the constituent structural elements due to the manufacturing easiness. Whereas, recent advanced technologies open up a space to exploit different material for the microstructural elements along with different geometries and it is shown that unprecedented properties can be achieved considering multi-material microstructural design [7]. Though the analytical investigations are still limited in literature for the multilateral lattices. In this work, we proposed generalised analytical expressions for the equivalent elastic properties of the heterogeneous hexagonal lattice.

The material and geometric properties of the periodic unit cell dictates the mechanical properties of the micro-architected materials [8–10]. Several researchers proposed designs for obtaining a novel class of metamaterials with user-defined properties. The honeycomb material is being studied in an extensive manner [11–18] and utilised to manufacture structural members in the aerospace industry due to their high specific stiffness low relative density. It is also the geometric flexibility and manufacturing suitability that the hexagonal material is explored extensively. Researches have been performed to obtain different shapes for the unit cell such as rectangular, rhombus, re-entrant from the regular hexagonal material. In literature, we can find studies on analytical prediction of equivalent elastic moduli for regular as well as irregular hexagonal lattice [19–23]. All these analytical developments deal with single material lattice. Both material and geometric properties of constituent elements dictate the overall behaviour of the lattices and consequently, this opens up a significant opportunity to explore a wide range of designs. The unit cell approach is a widely used and acceptable approach to obtain the equivalent material behaviour of the whole lattice [24–29]. [There are also research works on the energy equivalence continuum-based approach to obtain the equivalent continuum properties of the lattice structures. In \[30\] Taylor series expansion for the displacements of the repeating cell was used in this context.](#)

Most of the works to obtain user defined novel equivalent material properties are carried out by exploring the geometric aspects of the repetitive unit cells or the microstructure. Keeping the material the same and only by changing the geometry is quite easy and suitable from the manufacturing point of view. It is noticed in the literature that different geometry for the microstructure expands the design space for mechanical metamaterials and increase the scope for multi-functionality. The possibility to expand the multi-functional design space further with the help of additive manufacturing using different constituent materials along with the suitable geometry has been described in some of the recent literature [31–33]. Most of the works for the multifunctional materials are based on the numerically implemented inverse design methodology to predict the intrinsic

materials and their volume fractions [34, 35]. Though several analytical formulations for the equivalent elastic properties had been reported for hexagonal structure, investigation of the heterogeneous lattices are much limited. Recently, an analytical study is performed on anisotropic tailoring of multi-material lattices considering only the bending deformation of the constituent beam members [36]. Our present work addresses the analytical prediction and detailed study of all the equivalent elastic properties for multilateral lattice considering both bending and axial deformation.

In this work, we focus on the development of analytical expressions for the equivalent elastic properties of heterogeneous hexagonal lattices by exploiting the stiffness components of the constituent members. These expressions are more general as one can obtain the special case of classical homogeneous hexagonal lattice [2]. The formulation can also be utilised to obtain other geometries as well as auxetic case easily. This analysis addresses the contribution from axial stretching of the constituent elements along with bending. The generalised formulation is then used to get the expressions for thin and thick beams considering the Euler Bernoulli and Timoshenko beam theory respectively. heterogeneous lattices can help in expanding the design space for hexagonal lattices for tuning the material properties as per engineering requirements and the developed closed-form solutions can be utilized as a benchmark solution for further studies. The paper is organised as follows. In Section 2, the generalized formulation of the equivalent material properties for heterogeneous lattice is derived. The formulation can capture different geometric parameters for all the constituent beams. Next, The closed-form expressions are utilised to obtain those material properties considering Euler Bernoulli beam theory which is applicable for lattice with thin beams. Various cases are discussed such as the most general one that is all the material and geometric properties of a constituent element are different, multi-material but same wall thickness and same material but different wall thickness are discussed in Section 3. The analytical formulation is extended for thick beam configurations considering the Timoshenko beam theory and illustrated in Section 4. The results corresponding to the different cases are obtained and discussed in Section 6. Finally, the conclusions are drawn in Section 7.

2. Equivalent elastic properties of heterogeneous lattices

In this section, the generalized expressions for the equivalent elastic properties of the heterogeneous lattice are derived. The equivalent elastic property of a lattice structure are obtained by exploiting the periodicity of a suitably selected unit cell. The representative example of a hexagonal heterogeneous lattice and its corresponding unit cell is shown in Fig. 1. The entire lattice can be constructed by tessellating the representative unit cell in both directions. We consider the effect of both bending and stretching of the cell walls under the application of in-plane tensile/compressive stresses. The constitutive element of the unit cell in Fig. 1(b) can be modelled as a beam under the uniform applied stress in the out-of-plane direction. Fig. 1(c) shows a schematic of a two noded general beam element with six degrees of freedom. In the following subsections, a general derivation of the equivalent elastic properties of the heterogeneous lattice are obtained using the principle of structural mechanics by exploiting the stiffness coefficients of the constitutive beam elements.

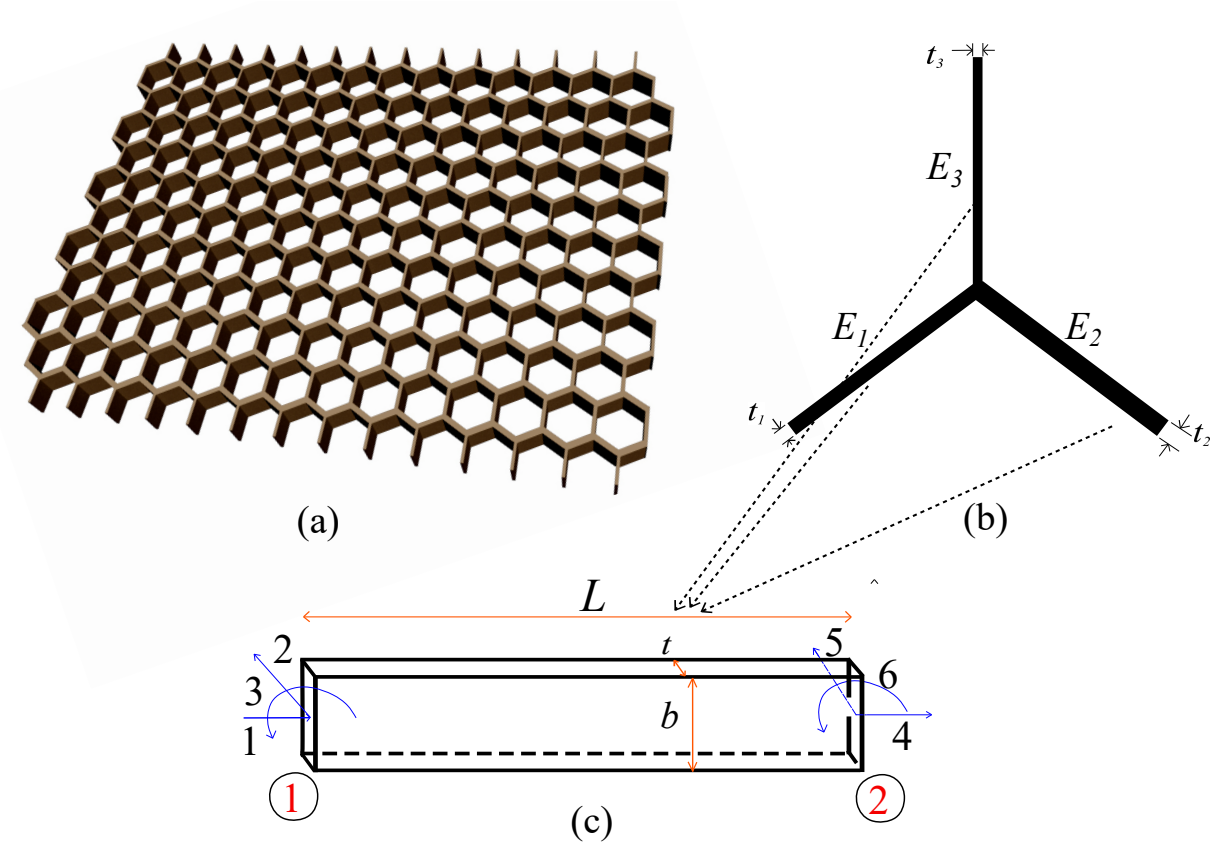


Fig. 1: (a) Illustration of a hexagonal heterogeneous lattice material (b) The unit cell used for the heterogeneous lattice with thickness t_1 , t_2 and t_3 and Young's modulus E_1 , E_2 and E_3 for different beam members (c) A representative two noded beam element with three degrees of freedom (corresponds to the axial, transverse and rotational deformation) at each node.

2.1. The longitudinal Young's modulus \bar{E}_1

A uniform stress field σ_1 is applied to the unit cell in direction-1 as shown in Fig. 2 to derive the expression of the equivalent longitudinal Young's modulus. This results in a force P being applied at point A and B on the unit cell. The magnitude of the force P is given by

$$P = \sigma_1 b(h + l \sin \theta) \quad (1)$$

Considering η and γ as deformations transverse and along the inclined member AO and BO we have

$$\eta_A = \frac{P \sin \theta}{K_{55}^a} \quad \text{and} \quad \gamma_A = \frac{P \cos \theta}{K_{44}^a} \quad (2)$$

$$\eta_B = \frac{P \sin \theta}{K_{55}^b} \quad \text{and} \quad \gamma_B = \frac{P \cos \theta}{K_{44}^b} \quad (3)$$

Here K_{55}^i and K_{44}^i ($i = a$ and b) are elements of the stiffness matrix of the inclined member AO and BO of length l . The deflection in the 1-direction of point A and B are therefore

$$\delta_{1A} = \eta_A \sin \theta + \gamma_A \cos \theta = P \left(\frac{\sin^2 \theta}{K_{55}^a} + \frac{\cos^2 \theta}{K_{44}^a} \right) = \frac{P \sin^2 \theta}{K_{55}^a} \left(1 + \cot^2 \theta \frac{K_{55}^a}{K_{44}^a} \right) \quad (4)$$

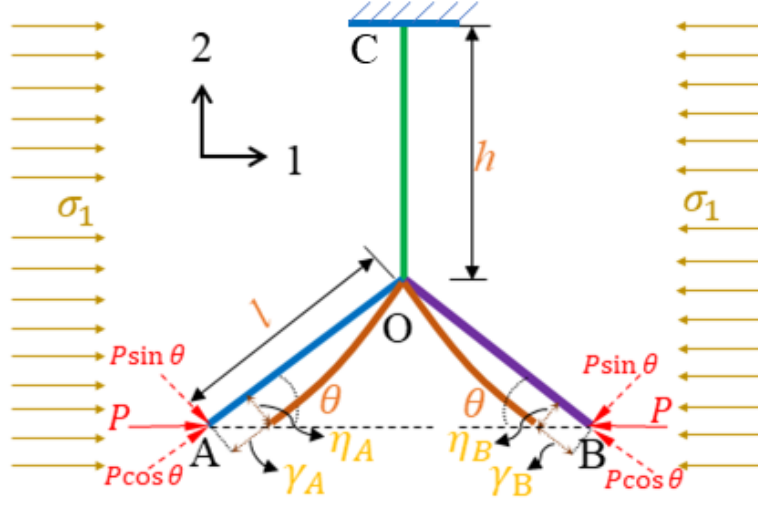


Fig. 2: Schematic diagram of a unit cell and deformation patterns under the application of a uniform stress field σ_1 in the 1-direction. This configuration is used to derive the expression of the longitudinal Young's modulus \bar{E}_1 and Poisson's ratio ν_{12} .

and

$$\delta_{1B} = \eta_B \sin \theta + \gamma_B \cos \theta = P \left(\frac{\sin^2 \theta}{K_{55}^b} + \frac{\cos^2 \theta}{K_{44}^b} \right) = \frac{P \sin^2 \theta}{K_{55}^b} \left(1 + \cot^2 \theta \frac{K_{55}^b}{K_{44}^b} \right) \quad (5)$$

The total deflection in 1-direction is

$$\delta_1 = \delta_{1A} + \delta_{1B} = P \left(\sin^2 \theta \left(\frac{1}{K_{55}^a} + \frac{1}{K_{55}^b} \right) + \cos^2 \theta \left(\frac{1}{K_{44}^a} + \frac{1}{K_{44}^b} \right) \right) \quad (6)$$

The strain the 1-direction is obtained as

$$\epsilon_1 = \frac{\delta_1}{2l \cos \theta} = \frac{P \left(\sin^2 \theta \left(\frac{1}{K_{55}^a} + \frac{1}{K_{55}^b} \right) + \cos^2 \theta \left(\frac{1}{K_{44}^a} + \frac{1}{K_{44}^b} \right) \right)}{2l \cos \theta} \quad (7)$$

Using this, the Young's modulus in 1-direction is obtained in terms of the elements of the stiffness matrix as

$$\bar{E}_1 = \frac{\sigma_1}{\epsilon_1} = \frac{2 \cos \theta}{b(\beta + \sin \theta) \sin^2 \theta \left(\left(\frac{1}{K_{55}^a} + \frac{1}{K_{55}^b} \right) + \cot^2 \theta \left(\frac{1}{K_{44}^a} + \frac{1}{K_{44}^b} \right) \right)} \quad (8)$$

From Eq. (8), it can be observed that for the inclined members only two coefficients, K_{55}^i and K_{44}^i ($i = a, b$), contribute towards the value of E_1 . In Subsection 2.2, the Poisson's ratio ν_{12} , will be derived. It can be noted that no assumptions are necessary for the displacement condition at point O or the member OC.

2.2. The Poisson's ratio ν_{12}

The Poisson's ratio ν_{12} is obtained considering the strain in the direction 2 for applied stress in the 1-direction from Fig. 2. The total deflection in the 2-direction is

$$-\delta_2 = -\delta_{2a} - \delta_{2b} \quad (9)$$

where,

$$-\delta_{2a} = \eta_A \cos \theta - \gamma_A \sin \theta = P \left(\frac{\sin \theta \cos \theta}{K_{55}^a} - \frac{\sin \theta \cos \theta}{K_{44}^a} \right) \quad (10)$$

and

$$-\delta_{2b} = \eta_B \cos \theta - \gamma_B \sin \theta = P \left(\frac{\sin \theta \cos \theta}{K_{55}^b} - \frac{\sin \theta \cos \theta}{K_{44}^b} \right) \quad (11)$$

The total strain in the 2-direction is

$$-\epsilon_2 = \frac{\delta_2}{2(h + l \sin \theta)} = \frac{\sin \theta \cos \theta \left(\left(\frac{1}{K_{55}^a} + \frac{1}{K_{55}^b} \right) - \left(\frac{1}{K_{44}^a} + \frac{1}{K_{44}^b} \right) \right)}{2(h + l \sin \theta)} \quad (12)$$

Using the expressions of the strains in directions 1 and 2 given by Eqs. (7) and (12), we obtain the Poisson's ratio ν_{12}

$$\nu_{12} = -\frac{\epsilon_2}{\epsilon_1} = \frac{\sin \theta \cos^2 \theta \left(\left(\frac{1}{K_{55}^a} + \frac{1}{K_{55}^b} \right) - \left(\frac{1}{K_{44}^a} + \frac{1}{K_{44}^b} \right) \right)}{(\beta + \sin \theta) \left(\sin^2 \theta \left(\frac{1}{K_{55}^a} + \frac{1}{K_{55}^b} \right) + \cos^2 \theta \left(\frac{1}{K_{44}^a} + \frac{1}{K_{44}^b} \right) \right)} \quad (13)$$

From equation (13), it can be observed that only two coefficients, K_{55} and K_{44} , contribute towards the value of ν_{12} .

2.3. The transverse Young's modulus \bar{E}_2

The transverse Young's modulus is derived by considering a uniform stress field σ_2 applied to the unit cell in direction-2 as shown in Fig. 3. The total vertical force W

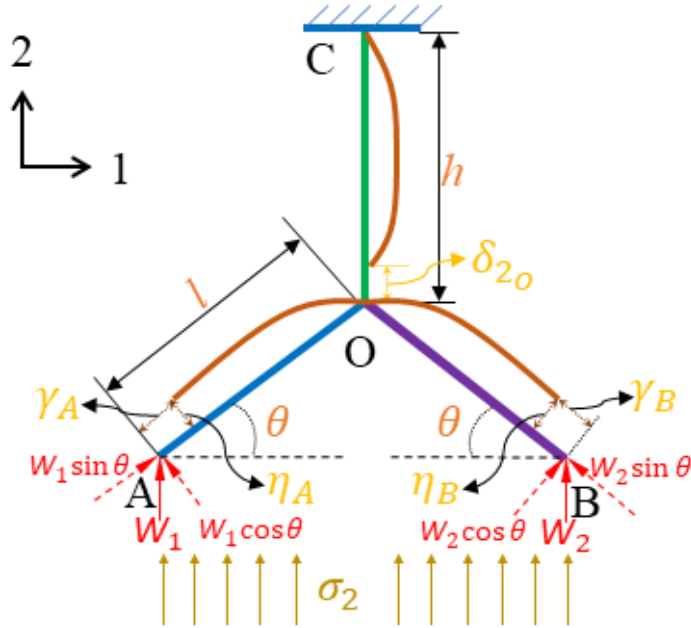


Fig. 3: Schematic diagram of a unit cell and deformation patterns under the application of uniform stress field σ_2 applied in the 2-direction. This configuration is used to derive the expression of the longitudinal Young's modulus \bar{E}_2 and Poisson's ratio ν_{21} .

on the unit cell is distributed on the two constituent beam members according to their

stiffness values. Due to the displacement compatibility condition, the deformation of point A and B in the 2- direction are the same. Besides, the point O deflects only in the 2-direction. For the clarity of presentation, the deflection of the point A or B and point O are considered separately in the derivation and also shown separately in Fig. 3. The magnitude of this vertical force is given by

$$W = W_1 + W_2 = 2\sigma_2 bl \cos \theta \quad (14)$$

Considering η_A and γ_A as deformations transverse and along the inclined member AO , we have

$$\eta_A = \frac{W_1 \cos \theta}{K_{55}^a} \quad \text{and} \quad \gamma_A = \frac{W_1 \sin \theta}{K_{44}^a} \quad (15)$$

Similarly, the axial and transverse deformations of member BO are

$$\eta_B = \frac{W_2 \cos \theta}{K_{55}^b} \quad \text{and} \quad \gamma_B = \frac{W_2 \sin \theta}{K_{44}^b} \quad (16)$$

The deflection in the 2-direction of point A and point B are therefore

$$\delta_{2A} = \eta_A \cos \theta + \gamma_A \sin \theta = W_1 \left(\frac{\cos^2 \theta}{K_{55}^a} + \frac{\sin^2 \theta}{K_{44}^a} \right) \quad (17)$$

and

$$\delta_{2B} = \eta_B \cos \theta + \gamma_B \sin \theta = W_2 \left(\frac{\cos^2 \theta}{K_{55}^b} + \frac{\sin^2 \theta}{K_{44}^b} \right) \quad (18)$$

The total force acting in the 2-direction at point O is W . Therefore, point O only has a deformation in the 2-direction due to the axial deformation δ_{2O} of the vertical member OC

$$\delta_{2O} = \frac{W}{K_{44}^{(h)}} \quad (19)$$

The assumed compatibility condition is given by

$$\delta_{2A} = \delta_{2B} \quad (20)$$

Putting the values of δ_{2B} and δ_{2A} in Eq. (20) and performing some algebraic manipulations we obtain

$$W_1 = \frac{W \left(\frac{\cos^2 \theta}{K_{55}^b} + \frac{\sin^2 \theta}{K_{44}^b} \right)}{\left(\cos^2 \theta \left(\frac{1}{K_{55}^a} + \frac{1}{K_{55}^b} \right) + \sin^2 \theta \left(\frac{1}{K_{44}^a} + \frac{1}{K_{44}^b} \right) \right)} = \frac{W \hat{b}}{\hat{a} + \hat{b}} \quad (21)$$

$$\text{and} \quad W_2 = \frac{W \left(\frac{\cos^2 \theta}{K_{55}^a} + \frac{\sin^2 \theta}{K_{44}^a} \right)}{\left(\cos^2 \theta \left(\frac{1}{K_{55}^a} + \frac{1}{K_{55}^b} \right) + \sin^2 \theta \left(\frac{1}{K_{44}^a} + \frac{1}{K_{44}^b} \right) \right)} = \frac{W \hat{a}}{\hat{a} + \hat{b}} \quad (22)$$

where

$$\hat{a} = \frac{\cos^2 \theta}{K_{55}^a} + \frac{\sin^2 \theta}{K_{44}^a} \quad (23)$$

$$\text{and } \hat{b} = \frac{\cos^2 \theta}{K_{55}^b} + \frac{\sin^2 \theta}{K_{44}^b} \quad (24)$$

Here $(\bullet)^{(h)}$ corresponds to the properties arising from the vertical member OC of length h .

The total deflection in the 2-direction is obtained as

$$\delta_2 = \frac{\delta_{2A} + \delta_{2B}}{2} + \delta_{2O} = W \left(\frac{\hat{a}\hat{b}}{(\hat{a} + \hat{b})} + \frac{1}{K_{44}^h} \right) \quad (25)$$

The strain in the 2-direction is therefore

$$\epsilon_2 = \frac{\delta_2}{h + l \sin \theta} = \frac{2\sigma_2 l b \cos \theta \left(\frac{\hat{a}\hat{b}}{(\hat{a} + \hat{b})} + \frac{1}{K_{44}^h} \right)}{h + l \sin \theta} \quad (26)$$

Using this, the Young's modulus in 1-direction is derived in terms of the elements of the stiffness matrix as

$$\bar{E}_2 = \frac{\sigma_2}{\epsilon_2} = \frac{(\beta + \sin \theta)}{2b \cos \theta \left(\frac{\hat{a}\hat{b}}{(\hat{a} + \hat{b})} + \frac{1}{K_{44}^h} \right)} \quad (27)$$

From Eqs. (23), (24) and (27), it can be observed that only two coefficients of the 6×6 element stiffness matrix of the inclined member and one coefficients of the 6×6 element stiffness matrix of vertical member, namely, K_{55} , K_{44} and $K_{44}^{(h)}$, contribute towards the value of E_2 . The Poisson's ratio corresponding to this stress field, namely ν_{21} , is derived in 2.4.

2.4. The Poisson's ratio ν_{21}

To obtain the Poisson's ratio ν_{21} , we need to obtain the strain in the direction 1 due to the applied stress in the 2-direction (Fig. 3). The total deflection in the 1-direction is

$$\delta_1 = \gamma_A \cos \theta - \eta_A \sin \theta + \gamma_B \cos \theta - \eta_B \sin \theta \quad (28)$$

$$= \frac{W\hat{b}}{\hat{a} + \hat{b}} \sin \theta \cos \theta \left(\frac{1}{K_{44}^a} - \frac{1}{K_{55}^a} \right) + \frac{W\hat{a}}{\hat{a} + \hat{b}} \sin \theta \cos \theta \left(\frac{1}{K_{44}^b} - \frac{1}{K_{55}^b} \right) \quad (29)$$

The total strain in the 1-direction is

$$\epsilon_1 = \frac{\delta_1}{2l \cos \theta} \quad (30)$$

Using the expressions of the strains in directions 1 and 2 given by Eqs. (26) and (30), we obtain the Poisson's ratio ν_{21}

$$\nu_{21} = -\frac{\epsilon_1}{\epsilon_2} = \frac{(\beta + \sin \theta) \sin \theta \left(\hat{b} \left(\frac{1}{K_{55}^a} - \frac{1}{K_{44}^a} \right) + \hat{a} \left(\frac{1}{K_{55}^b} - \frac{1}{K_{44}^b} \right) \right)}{2(\hat{a} + \hat{b}) \left(\frac{\hat{a}\hat{b}}{(\hat{a} + \hat{b})} + \frac{1}{K_{44}^h} \right)} \quad (31)$$

From Eq. (31), it can be observed that only two coefficients of the 6×6 element stiffness matrix of the inclined member and one coefficients of the 6×6 element stiffness matrix of vertical member, namely, K_{55} , K_{44} and $K_{44}^{(h)}$, contribute towards the value ν_{21} .

2.5. The shear modulus \bar{G}_{21}

The expression for the shear modulus G_{12} is derived in this section considering the contribution of strains from bending and axial deformations. Figure 4 depicts the details of the forces and deformation patterns of both cases. For deriving the bending contributions,

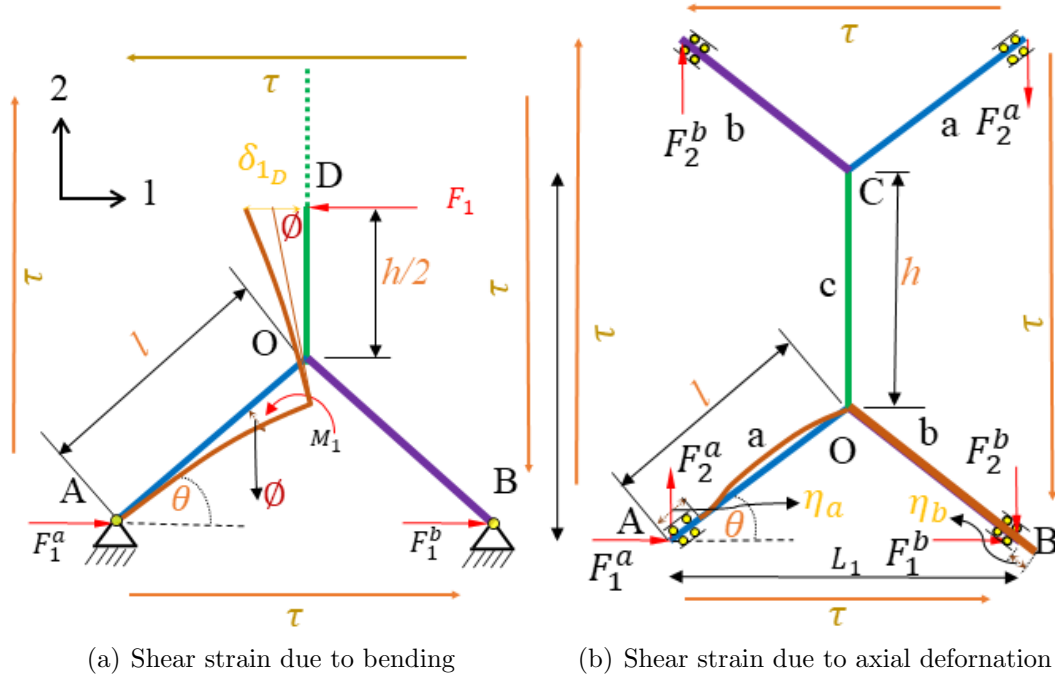


Fig. 4: Schematic of the deformation patterns and internal forces under the application of the shear stress field τ . These configurations are used to derive the expression of the shear modulus \bar{G}_{12} .

considering the deformation of the adjacent cells, it can be deduced that the midpoint of the vertical member will only have a deformation in the 1-direction due to shear. Therefore, in Fig. 4(a) unit cell with the vertical member with length $h/2$ and a slant member with length l are considered. Due to the symmetry points A and O will not have any relative movement. The shear deflection γ_D due to bending consists of bending deflection of the member OD and its deflection due to rotation of joint O arising from the bending of the slant members.

It can be noted here that the elements of the stiffness matrix (for example, refer to Eq. (67) later in the paper) will be different for the vertical member and the slant member due to their different lengths. The bending deformation of point D with respect to point O in the direction 1 can be obtained using the stiffness elements of the stiffness matrix with length $h/2$. The bending deformation η_D is described below.

$$\eta_D = \frac{F_1}{\left(K_{55}^{(h/2)} - \frac{K_{56}^{(h/2)} K_{65}^{(h/2)}}{K_{66}^{(h/2)}} \right)} = \frac{F_1 K_{66}^{(h/2)}}{\left(K_{55}^{(h/2)} K_{66}^{(h/2)} - \left(K_{56}^{(h/2)} \right)^2 \right)} \quad (32)$$

In the above

$$F_1 = 2\tau lb \cos \theta \quad (33)$$

and we make use of the symmetry of the elements of the stiffness matrix. Here $(\bullet)^{(h/2)}$ corresponds to the properties arising from the vertical member OD of length $h/2$ as shown in Fig. 4(a).

From the diagram in Fig. 4(a), the moment acting on point O is obtained as

$$M = F_1 \times \frac{h}{2} = \frac{F_1 h}{2} = M_1 + M_2 \quad (34)$$

The rotations of the two adjacent beams at point O are the same. On the basis of the degrees of freedom as denoted in Section 2 (Fig. 1 (c)), deflection of the end O with respect to the end A due to application of moment M at the end O is given as

$$\delta_{r_1} = \frac{M_1}{-K_{65}^a} = \delta_{r_2} = \frac{M_2}{-K_{65}^b} \quad (35)$$

Here K_{65} denotes the stiffness element corresponding to the slant member. The negative sign emerges due to the direction of the rotation as given in Fig. 1 (c). The values of M_1 and M_2 are given by

$$M_1 = M \frac{K_{65}^a}{K_{65}^a + K_{65}^b} \quad (36)$$

$$\text{and } M_2 = M \frac{K_{65}^b}{K_{65}^a + K_{65}^b} \quad (37)$$

Thus the rotation of joint O can be expressed as

$$\phi = \phi_1 = \phi_2 = \frac{\delta_{r_1}}{l} = -\frac{M_1}{lK_{65}^a} = -\frac{K_{65}^a}{K_{65}^a + K_{65}^b} \frac{M}{lK_{65}^a} = -\frac{F_1 h}{2l(K_{65}^a + K_{65}^b)} \quad (38)$$

The shear deformation in the 1-direction due to bending at point D under the application of shear stress τ can be expressed as

$$\begin{aligned} \delta_{1D} &= 2 \left(\phi \frac{h}{2} + \eta_D \right) \\ &= -\frac{F_1 h^2}{2l(K_{65}^a + K_{65}^b)} + \frac{2F_1 K_{66}^{(h/2)}}{\left(K_{55}^{(h/2)} K_{66}^{(h/2)} - \left(K_{56}^{(h/2)} \right)^2 \right)} \end{aligned} \quad (39)$$

The factor 2 in the above expression arises due to the consideration of two units shown in Fig. 4(b) to capture the total shear deformation by representing a complete unit cell that can create the entire lattice structure on tessellation.

To obtain the shear deformation due to axial stretching deformation, we consider the forcing F_1 in (33) and F_2 as given by

$$F_2 = \tau b(h + 2l \sin \theta) \quad (40)$$

To calculate the forces acting on the member a and b due to F_1 , we consider the description in Fig. 4(b). The force F_1 will be distributed between the two members as per their stiffness. This configuration is analogous to a parallel spring system. The compatibility condition is that the displacements of the members a and b in the 1-direction are the same. The total axial deformations of AO is $\eta_a = \eta_a^{F_1} + \eta_a^{F_2}$ and for BO it is $\eta_b = \eta_b^{F_1} + \eta_b^{F_2}$. The

axial deformation of AO and BO due to F_1^a and F_1^b are

$$\eta_a^{F_1} = \frac{F_1^a \cos \theta}{K_{44}^a} \quad (41)$$

$$\text{and } \eta_b^{F_1} = \frac{F_1^b \cos \theta}{K_{44}^b} \quad (42)$$

The components of $\eta_a^{F_1}$ in 1 and 2 directions are

$$\delta_1^{F_1^a} = \eta_a^{F_1} \cos \theta = \frac{F_1^a \cos^2 \theta}{K_{44}^a} \quad \text{and} \quad \delta_2^{F_1^a} = \eta_a^{F_1} \sin \theta = \frac{F_1^a \sin \theta \cos \theta}{K_{44}^a} \quad (43)$$

Similarly, the components of $\eta_b^{F_1}$ in 1 and 2 directions are

$$\delta_1^{F_1^b} = \eta_b^{F_1} \cos \theta = \frac{F_1^b \cos^2 \theta}{K_{44}^b} \quad \text{and} \quad \delta_2^{F_1^b} = \eta_b^{F_1} \sin \theta = \frac{F_1^b \sin \theta \cos \theta}{K_{44}^b} \quad (44)$$

The compatibility condition is given by

$$\eta_a^{F_1} \cos \theta = \eta_b^{F_1} \cos \theta \quad (45)$$

From the force equilibrium one also has

$$F_1 = F_1^a + F_1^b \quad (46)$$

Considering Eqs. (45) and (46) we obtain the expressions for F_1 and F_2 as

$$F_1^a = F_1 \left(\frac{K_{44}^a}{K_{44}^a + K_{44}^b} \right) \quad \text{and} \quad F_1^b = F_1 \left(\frac{K_{44}^b}{K_{44}^a + K_{44}^b} \right) \quad (47)$$

To obtain the displacement contribution from the force F_2 , a similar approach is considered and it is described below.

To calculate the forces acting on the members a and b due to F_2 we consider Fig. 4(b). The two arms are acting as a parallel spring system and F_2 is getting distributed in the two members as per their stiffness. The compatibility condition here is that the displacements in the 2 direction are the same for members a and b . The axial deformation of BO and CD due to F_2^a and F_2^b are

$$\eta_a^{F_2} = \frac{F_2^a \sin \theta}{K_{44}^a} \quad (48)$$

$$\text{and } \eta_b^{F_2} = \frac{F_2^b \sin \theta}{K_{44}^b} \quad (49)$$

$$(50)$$

The components of $\eta_a^{F_2}$ in 1 and 2 directions are

$$\delta_1^{F_2^a} = \eta_a^{F_2} \cos \theta = \frac{F_2^a \sin \theta \cos \theta}{K_{44}^a} \quad \text{and} \quad \delta_2^{F_2^a} = \eta_a^{F_2} \sin \theta = \frac{F_2^a \sin^2 \theta}{K_{44}^a} \quad (51)$$

In the same manner, the components of $\eta_b^{F_2}$ in 1 and 2 directions are

$$\delta_1^{F_2^b} = \eta_b^{F_2} \cos \theta = \frac{F_2^b \sin \theta \cos \theta}{K_{44}^b} \quad \text{and} \quad \delta_2^{F_2^b} = \eta_b^{F_2} \sin \theta = \frac{F_2^b \sin^2 \theta}{K_{44}^b} \quad (52)$$

The compatibility condition is given as

$$\eta_a^{F_2} \sin \theta = \eta_b^{F_2} \sin \theta \quad (53)$$

From the force equilibrium, one obtains

$$F_2 = F_2^a + F_2^b \quad (54)$$

Considering Eqs. (53) and (54) we obtain the expressions for F_1 and F_2 as

$$F_2^a = F_2 \left(\frac{K_{44}^a}{K_{44}^a + K_{44}^b} \right) \quad \text{and} \quad F_2^b = F_2 \left(\frac{K_{44}^b}{K_{44}^a + K_{44}^b} \right) \quad (55)$$

The lengths of the unit cell in Fig. 4(b) in the 1 and 2 directions are given by

$$L_1 = 2l \cos \theta \quad (56)$$

$$\text{and} \quad L_2 = (h + l \sin \theta) \quad (57)$$

Total deflections on 1 and 2 directions will consist of the deflection of AO and BO due to F_1 and F_2 . The expressions are as follows

$$\delta_1 = \delta_1^{F_1} + \delta_1^{F_2} = \eta_a^{F_1} \cos \theta + \eta_a^{F_2} \cos \theta + \eta_b^{F_2} \cos \theta \quad (58)$$

$$\begin{aligned} &= \frac{F_1 \cos^2 \theta}{K_{44}^a + K_{44}^b} + \sin \theta \cos \theta \left(\frac{F_2^a}{K_{44}^a} + \frac{F_2^b}{K_{44}^b} \right) = \frac{F_1 \cos^2 \theta}{K_{44}^a + K_{44}^b} + \frac{2F_2 \sin \theta \cos \theta}{K_{44}^a + K_{44}^b} \\ &= \frac{\tau l b \cos \theta}{K_{44}^a + K_{44}^b} (2 \cos^2 \theta + 2(\beta + 2 \sin \theta) \sin \theta) \end{aligned} \quad (59)$$

$$\begin{aligned} \delta_2 &= \delta_2^{F_1} + 2\delta_2^{F_2} = \eta_a^{F_1} \sin \theta + \eta_b^{F_1} \sin \theta + 2\eta_b^{F_2} \sin \theta \\ &= \sin \theta \cos \theta \left(\frac{F_1^a}{K_{44}^a} + \frac{F_1^b}{K_{44}^b} \right) + \frac{2F_2 \sin^2 \theta}{K_{44}^a + K_{44}^b} = \frac{2F_1 \sin \theta \cos \theta}{K_{44}^a + K_{44}^b} + \frac{2F_2 \sin^2 \theta}{K_{44}^a + K_{44}^b} \\ &= \frac{\tau l b \sin \theta}{K_{44}^a + K_{44}^b} (4 \cos^2 \theta + 2(\beta + 2 \sin \theta) \sin \theta) \end{aligned} \quad (60)$$

The total shear strain arising due to bending and axial deformation is given by

$$\begin{aligned} \gamma &= \frac{\delta_1 + \delta_{1D}}{L_2} + \frac{\delta_2}{L_1} = \frac{\delta_1 + \delta_{1D}}{h + l \sin \theta} + \frac{\delta_2}{2l \cos \theta} \\ &= \underbrace{\frac{\delta_{1D}}{h + l \sin \theta}}_{\gamma_b} + \underbrace{\frac{\delta_1}{h + l \sin \theta} + \frac{\delta_2}{2l \cos \theta}}_{\gamma_s} \end{aligned} \quad (61)$$

Here γ_b and γ_s are respectively the bending and stretching components of the total shear strain.

Now using Eq. (39) we obtain the bending component of the shear strain as

$$\begin{aligned}
\gamma_b &= \frac{\delta_{1D}}{(h + l \sin \theta)} \\
&= \frac{F_1}{(h + l \sin \theta)} \left(-\frac{h^2}{2l(K_{65}^a + K_{65}^b)} + \frac{2K_{66}^{(h/2)}}{\left(K_{55}^{(h/2)} K_{66}^{(h/2)} - \left(K_{56}^{(h/2)} \right)^2 \right)} \right) \\
&= \frac{\tau b \cos \theta}{(\beta + \sin \theta)} \left(-\frac{h^2}{l(K_{65}^a + K_{65}^b)} + \frac{4K_{66}^{(h/2)}}{\left(K_{55}^{(h/2)} K_{66}^{(h/2)} - \left(K_{56}^{(h/2)} \right)^2 \right)} \right)
\end{aligned} \tag{62}$$

The stretching component of the shear strain can be simplified as

$$\begin{aligned}
\gamma_s &= \frac{\delta_1}{h + l \sin \theta} + \frac{\delta_2}{2l \cos \theta} \\
&= \frac{2\tau b \cos \theta}{(\beta + 2 \sin \theta)(K_{44}^a + K_{44}^b)} (\cos^2 \theta + (\beta + \sin \theta) \sin \theta) \\
&\quad + \frac{\tau b \sin \theta}{2 \cos \theta (K_{44}^a + K_{44}^b)} (4 \cos^2 \theta + 2(\beta + 2 \sin \theta) \sin \theta)
\end{aligned} \tag{63}$$

Substituting the expressions of both the shear strains, the modulus can be obtained as

$$\begin{aligned}
\bar{G}_{12} &= \frac{\tau}{\gamma} = \frac{\tau}{\gamma_b + \gamma_s} \\
&= \frac{1}{\frac{b \cos \theta}{(\beta + \sin \theta)} \left(-\frac{h^2}{l(K_{65}^a + K_{65}^b)} + \frac{4K_{66}^{(h/2)}}{\left(K_{55}^{(h/2)} K_{66}^{(h/2)} - \left(K_{56}^{(h/2)} \right)^2 \right)} \right)} \\
&\quad + \frac{2b \cos \theta}{(\beta + \sin \theta)(K_{44}^a + K_{44}^b)} (\cos^2 \theta + (\beta + 2 \sin \theta) \sin \theta) \\
&\quad + \frac{b \sin \theta}{2 \cos \theta (K_{44}^a + K_{44}^b)} (4 \cos^2 \theta + 2(\beta + 2 \sin \theta) \sin \theta)
\end{aligned} \tag{64}$$

It can be observed from Eq. (64) that two different stiffness matrices contribute to the shear modulus which include stiffness terms K_{65} and K_{44} of the inclined member. Additionally, stiffness terms $K_{55}^{(h/2)}$, $K_{56}^{(h/2)}$ and $K_{66}^{(h/2)}$ of the vertical member with half the length also contribute to the shear modulus.

3. Heterogeneous lattices with thin walls

3.1. The stiffness matrix: Euler-Bernoulli beam theory

Euler Bernoulli beam theory is suitable to model constituent beam with thin walls ($\alpha < 0.1$). The governing equation of the transverse deflection for an Euler-Bernoulli beam [37] is given by

$$EI \frac{\partial^4 w}{\partial x^4} = f_b \tag{65}$$

Here $w \equiv w(x)$ and $f_b \equiv f_b(x)$ are the transverse displacement and applied transverse forcing on the beam. EI denote the bending stiffness, I is the area moment of inertia of the beam cross section and E is the Young's modulus of the beam material. The equation governing considering the axial deformation is as follows

$$EA \frac{\partial^2 u}{\partial x^2} = f_a \quad (66)$$

where $u \equiv u(x)$ and $f_x \equiv f_x(x)$ are the axial displacement and applied axial forcing on the beam respectively. EA depicts the axial stiffness of the beam and A is the cross sectional area of the beam. Finite element formulation with cubic shape function for the bending and linear shape function for the axial deformation can exactly represent the above force-displacement relationship of a beam element. The beam element has three degrees of freedom in each node, which correspond to axial, transverse and rotational deformations. The expression for the stiffness matrix [37, 38] of the beam element is

$$\mathbf{K}_{ij} = \begin{bmatrix} \frac{EA}{L} & 0 & 0 & -\frac{EA}{L} & 0 & 0 \\ 0 & \frac{12EI}{L^3} & \frac{6EI}{L^2} & 0 & -\frac{12EI}{L^3} & \frac{6EI}{L^2} \\ 0 & \frac{6EI}{L^2} & \frac{4EI}{L} & 0 & -\frac{6EI}{L^2} & \frac{2EI}{L} \\ -\frac{EA}{L} & 0 & 0 & \frac{EA}{L} & 0 & 0 \\ 0 & -\frac{12EI}{L^3} & -\frac{6EI}{L^2} & 0 & \frac{12EI}{L^3} & -\frac{6EI}{L^2} \\ 0 & \frac{6EI}{L^2} & \frac{2EI}{L} & 0 & -\frac{6EI}{L^2} & \frac{4EI}{L} \end{bmatrix} \quad (67)$$

Here $i, j = 1, \dots, 6$ denotes the entries corresponding to the degrees of freedom and shown in Fig. 1 (c). The entries of the stiffness matrix corresponding to for $i, j = 1$ and 4 correspond to the axial deformation governed by Eq. (66), while the entries for $i, j = 2, 3, 5$ and 6 correspond to the bending deformation governed by Eq. (65). The elements of the stiffness matrix will be used for both the inclined member ($L = l$) and the vertical member ($L = h$) in the unit cell.

3.2. The equivalent elastic properties: The general case

This section deals with the generalized formulation of equivalent elastic moduli considering beam with rectangular cross section. The expressions for the moment of inertia and the cross sectional area appears in the Eq. 67 are as follows

$$I = \frac{1}{12}bt^3 \quad \text{and} \quad A = bt \quad (68)$$

We define the following non-dimensional geometric parameters

$$\alpha = \frac{t}{l} \quad \text{and} \quad \beta = \frac{h}{l} \quad (69)$$

From the derivations in Subsection 2.1 and Subsection 2.3, it can be observed that two coefficients of the 6×6 element stiffness matrix of the inclined member and one coefficients of the 6×6 element stiffness matrix of vertical member, namely, K_{55} , K_{44} and $K_{44}^{(h)}$, are necessary to obtain E_1 , E_2 , ν_{12} and ν_{21} . The simplified expressions of moment of inertia

and the cross-sectional area in Eq. (68), the stiffness coefficients are given by

$$K_{55}^a = \frac{12E_1I_1}{l^3} = E_1b\alpha_1^3, K_{44}^a = \frac{E_1A_1}{l} = E_1b\alpha_1 \quad \text{and} \quad K_{44}^{(h)} = \frac{E_3A_3}{h} = \frac{E_3bt_3}{h} = \frac{E_3b\alpha_3}{\beta} \quad (70)$$

Using these stiffness coefficients, from Eqs. (8), (27), (13) and (31) we have the following closed-form expressions for the equivalent elastic properties

$$\bar{E}_1 = \frac{2 \cos \theta E_1 E_2 \alpha_1^3 \alpha_2^3}{(\beta + \sin \theta) \sin^2 \theta (E_2 \alpha_2^3 (1 + \alpha_1^2 \cot^2 \theta) + E_1 \alpha_1^3 (1 + \alpha_2^2 \cot^2 \theta))} \quad (71)$$

$$\bar{E}_2 = \frac{(\beta + \sin \theta)}{2 \cos \theta \left(\frac{\beta}{E_3 \alpha_3} + \frac{(1 + \alpha_1^2 \tan^2 \theta)(1 + \alpha_2^2 \tan^2 \theta) \cos^2 \theta}{E_1 \alpha_1^3 (1 + \alpha_2^2 \tan^2 \theta) + E_2 \alpha_2^3 (1 + \alpha_1^2 \tan^2 \theta)} \right)} \quad (72)$$

$$\nu_{12} = \frac{\cos^2 \theta (E_2 \alpha_2^3 (1 - \alpha_1^2) + E_1 \alpha_1^3 (1 - \alpha_2^2))}{(\beta + \sin \theta) \sin \theta (E_2 \alpha_2^3 (1 + \alpha_1^2 \cot^2 \theta) + E_1 \alpha_1^3 (1 + \alpha_2^2 \cot^2 \theta))} \quad (73)$$

$$\nu_{21} = \frac{(\beta + \sin \theta) \frac{E_3 \alpha_3}{\beta} \sin \theta ((1 + \alpha_1^2 \tan^2 \theta)(1 - \alpha_2^2) + (1 + \alpha_2^2 \tan^2 \theta)(1 - \alpha_1^2))}{\left(E_1 \alpha_1^3 (1 + \alpha_2^2 \tan^2 \theta) + E_2 \alpha_2^3 (1 + \alpha_1^2 \tan^2 \theta) + \cos^2 \theta (1 + \alpha_1^2 \tan^2 \theta)(1 + \alpha_2^2 \tan^2 \theta) \frac{E_3 \alpha_3}{\beta} \right)} \quad (74)$$

For the shear modulus, seven elements from two different stiffness matrices are necessary. They are four stiffness coefficients K_{65}^i and K_{44}^i with $K_{65}^i = -6 \frac{EI}{l^2} = -1/2 \frac{E_i b t_i^3}{l^2} = -1/2 E_i b \alpha_i^3 l$ from the inclined members. Where $i = a$ and b denotes the two inclined members. We also need three elements of the stiffness matrix of the vertical member mentioned below

$$K_{55}^{(h/2)} = \frac{12E_3I}{(h/2)^3} = \frac{8E_3b\alpha_3^3}{\beta^3}, K_{56}^{(h/2)} = -\frac{6E_3I}{(h/2)^2} = -\frac{2E_3b\alpha_3^3l}{\beta^2}, K_{66}^{(h/2)} = \frac{4E_3I}{(h/2)} = \frac{2E_3b\alpha_3^3l^2}{3\beta} \quad (75)$$

Using these expressions, from Eq. (64) we obtain

$$\bar{G}_{12} = \frac{1}{\frac{\cos \theta}{(\beta + \sin \theta) \left(\frac{2\beta^2}{(E_1 \alpha_1^3 + E_2 \alpha_2^3)} + \frac{2\beta^3}{E_3 \alpha_3^3} \right)} + \frac{2 \cos \theta (2 + \beta \sin \theta - \cos^2 \theta)}{(\beta + \sin \theta) (E_1 \alpha_1 + E_2 \alpha_2)} + \frac{\sin \theta (2 + \beta \sin \theta)}{\cos \theta (E_1 \alpha_1 + E_2 \alpha_2)}} \quad (76)$$

3.3. The equivalent elastic properties: Special cases

3.3.1. Heterogeneous lattices with single material and uniform wall thickness

This section deals with the closed-form expression of the hexagonal lattice with uniform wall thickness for all the constituent beam members and with the same material properties. The expressions are derived from the generalized expressions (see Eqs. (71), (72), (73),

(74) and (76)) considering $\alpha_1 = \alpha_2 = \alpha_3$ and $E_1 = E_2 = E_3$.

$$\bar{E}_1 = \frac{E\alpha^3 \cos \theta}{(\beta + \sin \theta) (\sin^2 \theta + \alpha^2 \cos^2 \theta)} \quad (77)$$

$$\bar{E}_2 = \frac{E\alpha^3(\beta + \sin \theta)}{(1 - \alpha^2) \cos^3 \theta + \alpha^2(2\beta + 1) \cos \theta} \quad (78)$$

$$\nu_{12} = \frac{(1 - \alpha^2) \sin \theta \cos^2 \theta}{(\beta + \sin \theta) (\sin^2 \theta + \alpha^2 \cos^2 \theta)} \quad (79)$$

$$\nu_{21} = \frac{(1 - \alpha^2) \sin \theta (\beta + \sin \theta)}{(1 - \alpha^2) \cos^2 \theta + \alpha^2(2\beta + 1)} \quad (80)$$

$$\text{and } \bar{G}_{12} = \frac{E\alpha^3(\beta + \sin \theta)}{(\beta^2(1 + 2\beta) + \alpha^2(\cos \theta + (\beta + \sin \theta) \tan \theta)^2) \cos \theta} \quad (81)$$

These expressions match exactly with reference [23]. The classical Gibson Ashby expressions for the equivalent material properties can be obtained considering $\alpha^2 \ll 1$ in the above expressions.

3.3.2. Heterogeneous lattices with single material but different wall thicknesses

This section presents the closed-form expressions of hexagonal lattice considering $E_1 = E_2 = E_3$ but for different α values for the constituent beam members. Substituting these in the generalised expressions (71), (72), (73), (74) and (76) we obtain

$$\bar{E}_1 = \frac{2 \cos \theta E \alpha_1^3 \alpha_2^3}{(\beta + \sin \theta) \sin^2 \theta (\alpha_2^3(1 + \alpha_1^2 \cot^2 \theta) + \alpha_1^3(1 + \alpha_2^2 \cot^2 \theta))} \quad (82)$$

$$\bar{E}_2 = \frac{E(\beta + \sin \theta)}{2 \cos \theta \left(\frac{\beta}{\alpha_3} + \frac{(1 + \alpha_1^2 \tan^2 \theta)(1 + \alpha_2^2 \tan^2 \theta) \cos^2 \theta}{\alpha_1^3(1 + \alpha_2^2 \tan^2 \theta) + \alpha_2^3(1 + \alpha_1^2 \tan^2 \theta)} \right)} \quad (83)$$

$$\nu_{12} = \frac{\cos^2 \theta (\alpha_2^3(1 - \alpha_1^2) + \alpha_1^3(1 - \alpha_2^2))}{(\beta + \sin \theta) \sin \theta (\alpha_2^3(1 + \alpha_1^2 \cot^2 \theta) + \alpha_1^3(1 + \alpha_2^2 \cot^2 \theta))} \quad (84)$$

$$\nu_{21} = \frac{\frac{\alpha_3}{\beta} \sin \theta ((1 + \alpha_1^2 \tan^2 \theta)(1 - \alpha_2^2) + (1 + \alpha_2^2 \tan^2 \theta)(1 - \alpha_1^2))}{\left(\alpha_1^3(1 + \alpha_2^2 \tan^2 \theta) + \alpha_2^3(1 + \alpha_1^2 \tan^2 \theta) + \cos^2 \theta (1 + \alpha_1^2 \tan^2 \theta)(1 + \alpha_2^2 \tan^2 \theta) \frac{\alpha_3}{\beta} \right)} \quad (85)$$

$$\text{and } \bar{G}_{12} = \frac{E}{\frac{\cos \theta}{(\beta + \sin \theta)} \left(\frac{2\beta^2}{(\alpha_1^3 + \alpha_2^3)} + \frac{2\beta^3}{\alpha_3^3} \right) + \frac{2 \cos \theta (2 + \beta \sin \theta - \cos^2 \theta)}{(\beta + \sin \theta) (\alpha_1 + \alpha_2)} + \frac{\sin \theta (2 + \beta \sin \theta)}{\cos \theta (\alpha_1 + \alpha_2)}} \quad (86)$$

3.3.3. Heterogeneous lattices with uniform wall thickness

In this section, we can find the expressions for the equivalent material properties of hexagonal lattice considering different material for constituent beam member of the unit cell keeping their thickness the same. The equations (71), (72), (73), (74) and (76) from

the generalized expressions are used to derive the following expressions

$$\bar{E}_1 = \frac{2E_1E_2\alpha^3 \cos \theta}{(\beta + \sin \theta) ((\sin^2 \theta + \alpha^2 \cos^2 \theta) (E_1 + E_2))} \quad (87)$$

$$\bar{E}_2 = \frac{(\beta + \sin \theta)}{2 \cos \theta \left(\frac{\beta}{E_3} + \frac{\cos^2 \theta (1 + \alpha^2 \tan^2 \theta)}{(E_1 + E_2)\alpha^2} \right)} \quad (88)$$

$$\nu_{12} = \frac{\cos^2 \theta (1 - \alpha^2)}{(\beta + \sin \theta)(1 + \alpha^2 \cot^2 \theta) \sin \theta} \quad (89)$$

$$\nu_{21} = \frac{2\alpha \frac{E_3\alpha}{\beta} (1 - \alpha^2)(\beta + \sin \theta) \sin \theta}{\alpha^3(E_1 + E_2) + \frac{E_3\alpha}{\beta} \cos^2 \theta (1 + \alpha^2 \tan^2 \theta)} \quad (90)$$

and

$$\begin{aligned} \bar{G}_{12} = & \frac{\alpha^3}{\frac{\cos \theta}{(\beta + \sin \theta)} \left(\frac{2\beta^2}{(E_1 + E_2)} + \frac{2\beta^3}{E_3} \right) + \frac{2 \cos \theta (2 + \beta \sin \theta - \cos^2 \theta) \alpha^2}{(\beta + \sin \theta) (E_1 + E_2)}} \\ & + \frac{\alpha^2 \sin \theta (2 + \beta \sin \theta)}{\cos \theta (E_1 + E_2)} \end{aligned} \quad (91)$$

Ignoring the axial stretching effect, that $\alpha^2 \ll 1$, these expressions match exactly with reference [36].

4. Heterogeneous lattices with thick walls

4.1. The stiffness matrix: Timoshenko beam theory

In this section, we discuss the closed-form solution for heterogeneous lattices and their special cases considering thick constituent beam members. The Euler-Bernoulli beam theory may lead to a higher error when the beams become thick. In this case, the Timoshenko beam theory can be used to obtain better results. [We can also find work on refined theory like direct asymptotic integration of the exact 3D problem of elasticity \[39\]. This is an advanced theory and there is a significant potential to exploit this in future studies.](#) In our analysis, we did not consider the effect of the junction of the three beam in a unit cell and due to this reason, the α value is not considered very high to avoid large errors in the numerical calculations. To understand the effect of the joint we refer to the work Malek and Gibson [40]. The governing equations for the transverse deflection [37] of a beam as per the Timoshenko beam theory are as follows

$$kAG \frac{\partial}{\partial x} \left(\frac{\partial w}{\partial x} - \theta \right) = 0 \quad \text{and} \quad EI \frac{\partial^2 \theta}{\partial x^2} + kAG \left(\frac{\partial w}{\partial x} - \theta \right) = f_b \quad (92)$$

Here $\theta \equiv \theta(x)$ is the rotation of the beam, kAG is the shear stiffness with G as the shear modulus and k is the shear coefficient. We consider solid rectangular sections with $k = 5/6$ for our studies. The stiffness matrix [37, 38] of the Timoshenko beam element

can be expressed as

$$\mathbf{K}_s = \begin{bmatrix} \frac{EA}{L} & 0 & 0 & -\frac{EA}{L} & 0 & 0 \\ 0 & 12 \frac{EI}{(1+\Phi)L^3} & 6 \frac{EI}{(1+\Phi)L^2} & 0 & -12 \frac{EI}{(1+\Phi)L^3} & 6 \frac{EI}{(1+\Phi)L^2} \\ 0 & 6 \frac{EI}{(1+\Phi)L^2} & \frac{(4+\Phi)EI}{(1+\Phi)L} & 0 & -6 \frac{EI}{(1+\Phi)L^2} & \frac{(2-\Phi)EI}{(1+\Phi)L} \\ -\frac{EA}{L} & 0 & 0 & \frac{EA}{L} & 0 & 0 \\ 0 & 12 \frac{EI}{(1+\Phi)L^3} & -6 \frac{EI}{(1+\Phi)L^2} & 0 & 12 \frac{EI}{(1+\Phi)L^3} & -6 \frac{EI}{(1+\Phi)L^2} \\ 0 & 6 \frac{EI}{(1+\Phi)L^2} & \frac{(2-\Phi)EI}{(1+\Phi)L} & 0 & -6 \frac{EI}{(1+\Phi)L^2} & \frac{(4+\Phi)EI}{(1+\Phi)L} \end{bmatrix} \quad (93)$$

The term Φ gives the relative importance of the shear deformations to the bending deformations. For a rectangular cross-section

$$\Phi = \frac{12EI}{kAGL^2} = \frac{2(1+\nu)}{k} \left(\frac{t}{L} \right)^2 \quad (94)$$

Here ν is the Poisson's ratio of the beam material and we have used the relationships

$$G = E/2(1+\nu) \quad (95)$$

$$I = \frac{1}{12}bt^3 \quad (96)$$

$$\text{and } A = bt \quad (97)$$

For beams with a length-to-depth ratio less than 5, has significant shear deformation effects. The stiffness matrix reduces to classical Euler-Bernoulli case for $\Phi = 0$. The Timoshenko beam model can be considered as a generalisation of the Euler-Bernoulli beam theory in the static regime.

The element stiffness matrix is obtained in Eq. (93) using the Timoshenko beam theory considers the shear deformation. To obtain the expressions of E_1 , E_2 , ν_{12} and ν_{21} the necessary stiffness coefficients are

$$K_{55}^i = \frac{12}{1+\Phi_i} \frac{E_i I_i}{l^3} = \frac{E_i b \alpha_i^3}{1+\Phi_i}, K_{44}^i = \frac{E_i A_i}{l} = E_i b \alpha_i \quad \text{and} \quad K_{44}^{(h)} = \frac{E_3 A_3}{h} = \frac{E_3 b \alpha_3}{\beta} \quad (98)$$

where from Eq. (94) we have

$$\Phi_i = \frac{2(1+\nu_i)}{k} \alpha_i^2 \quad (99)$$

where $i = a, b$. For the shear modulus, seven elements from two different stiffness matrices are necessary unlike the previous case. They are four coefficients of the 6×6 element stiffness matrix of the inclined members (K_{65}^i , K_{44}^i) as in (98). Their expressions for the coefficients are $K_{65}^i = -1/2 \frac{E_i b t_i^3}{l^2 (1+\Phi_i)} = -1/2 \frac{E_i b \alpha_i^3 l}{(1+\Phi_i)}$ ($i = a$ and b). The shear

correction factor for the vertical member can be obtained from Eq. (94) as

$$\Phi^{(h/2)} = \Phi_3 = \frac{2(1+\nu)}{k} \left(\frac{t}{h/2} \right)^2 = \frac{2(1+\nu)}{k} \frac{4\alpha_3^3}{\beta^2} \quad (100)$$

We other three elements of the stiffness matrix of the vertical member needed for the shear modulus are given by

$$\begin{aligned} K_{55}^{(h/2)} &= 8 \frac{E_3 b \alpha_3^3}{\beta^3} \left(\frac{1}{1 + \Phi_3} \right) \\ K_{56}^{(h/2)} &= -2 \frac{E_3 b \alpha_3^3 l}{\beta^2} \left(\frac{1}{1 + \Phi_3} \right) \\ \text{and } K_{66}^{(h/2)} &= \frac{E_3 b \alpha_3^3 l^2}{6\beta} \left(\frac{4 + \Phi_3}{1 + \Phi_3} \right) \end{aligned} \quad (101)$$

4.2. The equivalent elastic properties: The general case

This section deals with the most general case for the equivalent elastic properties of the heterogeneous hexagonal lattice considering thick beam assumption. Here, all the material properties and the thickness of the constituent beam members are considered as different and the generalized expressions are obtained from equations (8), (27), (13), (31) and (64) as

$$\bar{E}_1 = \frac{2 \cos \theta E_1 E_2 \alpha_1^3 \alpha_2^3}{(\beta + \sin \theta) \sin^2 \theta ((1 + \phi_1) E_2 \alpha_2^3 + (1 + \phi_2) E_1 \alpha_1^3 + \alpha_1^2 \alpha_2^2 \cot^2 \theta (E_1 \alpha_1 + E_2 \alpha_2))} \quad (102)$$

$$\bar{E}_2 = \frac{(\beta + \sin \theta)}{2 \cos \theta \left(\frac{\hat{a}\hat{b}}{(\hat{a} + \hat{b})} + \frac{\beta}{E_3 \alpha_3} \right)} \quad (103)$$

$$\nu_{12} = \frac{E_1 \alpha_1^3 (1 + \phi_2 - \alpha_2^2) + E_2 \alpha_2^3 (1 + \phi_1 - \alpha_1^2)}{\sin \theta (\beta + \sin \theta) (E_2 \alpha_2^3 (1 + \phi_1 + \alpha_1^2 \cot^2 \theta) + E_1 \alpha_1^3 (1 + \phi_2 + \alpha_2^2 \cot^2 \theta))} \quad (104)$$

$$\nu_{21} = \frac{(\beta + \sin \theta) \sin \theta \left(\hat{b} \frac{(1 + \phi_1 - \alpha_1^2)}{E_1 \alpha_1^3} + \hat{a} \frac{(1 + \phi_2 - \alpha_2^2)}{E_2 \alpha_2^3} \right)}{2(\hat{a} + \hat{b}) \left(\frac{\hat{a}\hat{b}}{(\hat{a} + \hat{b})} + \frac{\beta}{E_3 \alpha_3} \right)} \quad (105)$$

$$\begin{aligned} \text{and } \bar{G}_{12} &= \frac{1}{\frac{\cos \theta}{(\beta + \sin \theta)} \left(\frac{2\beta^2 (1 + \phi_1) (1 + \phi_2)}{E_3 \alpha_3^3 (2 + \phi_2 + \phi_1)} + \frac{\beta^3 (4 + \phi_3)}{2E_3 \alpha_3^3} \right)} \\ &+ \frac{2 \cos \theta (2 + \beta \sin \theta - \cos^2 \theta)}{(\beta + \sin \theta) (E_1 \alpha_1 + E_2 \alpha_2)} + \frac{\sin \theta (2 + \beta \sin \theta)}{\cos \theta (E_1 \alpha_1 + E_2 \alpha_2)} \end{aligned} \quad (106)$$

In the above, the expressions of \hat{a} and \hat{b} are defined as follows

$$\hat{a} = \frac{(1 + \Phi_1) \cos^2 \theta}{E_1 \alpha_1^3} \left(1 + \tan^2 \theta \frac{\alpha_1^2}{1 + \Phi_1} \right) \quad (107)$$

$$\text{and } \hat{b} = \frac{(1 + \Phi_2) \cos^2 \theta}{E_2 \alpha_2^3} \left(1 + \tan^2 \theta \frac{\alpha_2^2}{1 + \Phi_2} \right) \quad (108)$$

The above expressions are now utilised to obtain the following special cases.

4.3. The equivalent elastic properties: Special cases

4.3.1. Heterogeneous lattices with single material and uniform wall thickness

Using the generalized expressions (equations (102), (103), (104), (105) and (106)) we derive the expressions for the special case where the material and the thicknesses of the all constituent beam members are same. The equivalent elastic properties are given by

$$\bar{E}_1 = \frac{E \alpha^3 \cos \theta}{(\beta + \sin \theta) ((1 + \Phi) \sin^2 \theta + \alpha^2 \cos^2 \theta)} \quad (109)$$

$$\bar{E}_2 = \frac{E \alpha^3 (\beta + \sin \theta)}{(1 + \Phi - \alpha^2) \cos^3 \theta + \alpha^2 (2\beta + 1) \cos \theta} \quad (110)$$

$$\nu_{12} = \frac{\cos^2 \theta (1 + \Phi - \alpha^2)}{(\beta + \sin \theta) \sin \theta (1 + \Phi + \alpha^2 \cot^2 \theta)} \quad (111)$$

$$\nu_{21} = \frac{(\beta + \sin \theta) \sin \theta (1 + \Phi - \alpha^2)}{(1 + \Phi - \alpha^2) \cos^2 \theta + \alpha^2 (2\beta + 1)} \quad (112)$$

and

$$\bar{G}_{12} = \frac{E \alpha^3 (\beta + \sin \theta)}{(\beta^2 (1 + \Phi + 2\beta) + 8\beta\Phi + \alpha^2 (\cos \theta + (\beta + \sin \theta) \tan \theta)^2) \cos \theta} \quad (113)$$

These expressions match exactly with reference [23]. Substituting $\Phi = 0$, the equations derived here reduce to the corresponding Euler-Bernoulli case discussed in the previous section.

4.3.2. Heterogeneous lattices with single material but different wall thicknesses

Closed form expressions are obtained considering $E_1 = E_2 = E_3$ and different wall thickness for the constituent beam members in equations (102), (103), (104), (105) and (106). The equivalent elastic properties are given by

$$\bar{E}_1 = \frac{2 \cos \theta E \alpha_1^3 \alpha_2^3}{(\beta + \sin \theta) \sin^2 \theta ((1 + \phi_1) \alpha_2^3 + (1 + \phi_2) \alpha_1^3 + \alpha_1^2 \alpha_2^2 \cot^2 \theta (\alpha_1 + \alpha_2))} \quad (114)$$

$$\bar{E}_2 = \frac{(\beta + \sin \theta)}{2 \cos \theta \left(\frac{\hat{a}\hat{b}}{(\hat{a} + \hat{b})} + \frac{\beta}{E \alpha_3} \right)} \quad (115)$$

$$\nu_{12} = \frac{\alpha_1^3 (1 + \phi_2 - \alpha_2^2) + \alpha_2^3 (1 + \phi_1 - \alpha_1^2)}{\sin \theta (\beta + \sin \theta) (\alpha_2^3 (1 + \phi_1 + \alpha_1^2 \cot^2 \theta) + \alpha_1^3 (1 + \phi_2 + \alpha_2^2 \cot^2 \theta))} \quad (116)$$

$$\nu_{21} = \frac{(\beta + \sin \theta) \sin \theta \left(\hat{b} \frac{(1 + \phi_1 - \alpha_1^2)}{\alpha_1^3} + \hat{a} \frac{(1 + \phi_2 - \alpha_2^2)}{\alpha_2^3} \right)}{2(\hat{a} + \hat{b}) \left(\frac{\hat{a}\hat{b}}{(\hat{a} + \hat{b})} + \frac{\beta}{\alpha_3} \right)} \quad (117)$$

and $\bar{G}_{12} = \frac{E}{\frac{\cos \theta}{(\beta + \sin \theta)} \left(\frac{2\beta^2 (1 + \phi_1) (1 + \phi_2)}{\alpha_3^3 (2 + \phi_2 + \phi_1)} + \frac{\beta^3 (4 + \phi_3)}{2\alpha_3^3} \right) + \frac{2 \cos \theta (2 + \beta \sin \theta - \cos^2 \theta)}{(\beta + \sin \theta) (\alpha_1 + \alpha_2)} + \frac{\sin \theta (2 + \beta \sin \theta)}{\cos \theta (\alpha_1 + \alpha_2)}}$ (118)

where

$$\hat{a} = \frac{(1 + \Phi_1) \cos^2 \theta}{E \alpha_1^3} \left(1 + \tan^2 \theta \frac{\alpha_1^2}{1 + \Phi_1} \right) \quad (119)$$

$$\text{and } \hat{b} = \frac{(1 + \Phi_2) \cos^2 \theta}{E \alpha_2^3} \left(1 + \tan^2 \theta \frac{\alpha_2^2}{1 + \Phi_2} \right) \quad (120)$$

4.3.3. Heterogeneous lattices with uniform wall thickness

This subsection deals with lattice with different material properties for the constituent beam members but same thickness. The equivalent elastic properties are obtained from equations (102), (103), (104), (105) and (106).

$$\bar{E}_1 = \frac{2 \cos \theta E_1 E_2 \alpha^3}{(\beta + \sin \theta) \sin^2 \theta ((1 + \phi_1) E_2 + (1 + \phi_2) E_1 + \alpha^2 \cot^2 \theta (E_1 + E_2))} \quad (121)$$

$$\bar{E}_2 = \frac{(\beta + \sin \theta)}{2 \cos \theta \left(\frac{\hat{a}\hat{b}}{(\hat{a} + \hat{b})} + \frac{\beta}{E_3 \alpha} \right)} \quad (122)$$

$$\nu_{12} = \frac{E_1 \alpha^3 (1 + \phi_2 - \alpha^2) + E_2 \alpha^3 (1 + \phi_1 - \alpha^2)}{\sin \theta (\beta + \sin \theta) (E_2 \alpha^3 (1 + \phi_1 + \alpha^2 \cot^2 \theta) + E_1 \alpha^3 (1 + \phi_2 + \alpha^2 \cot^2 \theta))} \quad (123)$$

$$\nu_{21} = \frac{(\beta + \sin \theta) \sin \theta \left(\hat{b} \frac{(1 + \phi_1 - \alpha^2)}{E_1 \alpha^3} + \hat{a} \frac{(1 + \phi_2 - \alpha^2)}{E_2 \alpha^3} \right)}{2(\hat{a} + \hat{b}) \left(\frac{\hat{a}\hat{b}}{(\hat{a} + \hat{b})} + \frac{\beta}{E_3 \alpha} \right)} \quad (124)$$

and

$$\begin{aligned} \bar{G}_{12} = & \frac{\alpha^3}{\frac{\cos \theta}{(\beta + \sin \theta)} \left(\frac{2\beta^2 (1 + \phi_1) (1 + \phi_2)}{E_3 (2 + \phi_2 + \phi_1)} + \frac{\beta^3 (4 + \phi_3)}{2E_3} \right)} \\ & + \frac{2\alpha^2 \cos \theta (2 + \beta \sin \theta - \cos^2 \theta)}{(\beta + \sin \theta) (E_1 + E_2)} + \frac{\alpha^2 \sin \theta (2 + \sin \theta \beta)}{\cos \theta (E_1 + E_2)} \end{aligned} \quad (125)$$

In the above, the expressions of \hat{a} and \hat{b} are defined as follows

$$\hat{a} = \frac{(1 + \Phi_1) \cos^2 \theta}{E_1 \alpha^3} \left(1 + \tan^2 \theta \frac{\alpha^2}{1 + \Phi_1} \right) \quad (126)$$

$$\text{and } \hat{b} = \frac{(1 + \Phi_2) \cos^2 \theta}{E_2 \alpha^3} \left(1 + \tan^2 \theta \frac{\alpha^2}{1 + \Phi_2} \right) \quad (127)$$

In the next section, we validate the analytical expressions derived in the paper with independent finite element simulation results.

5. Finite element analysis of the lattice

The finite element (FE) validation of the closed form expressions is conducted in this section. The finite element model of the entire lattice is shown in Fig. 5(a). Figure 5(a) also shows the boundary condition and loading condition applied to the lattice for performing the finite element simulation. The commercial software NASTRAN has been used to obtain the FE results. The unit cell of the lattice is shown in Fig. 1(b). The details of the geometric parameters of the unit cell and the whole lattice used for the finite element analysis are shown in Table 1. Five different materials are used to create

Length (mm)	Thickness (mm)	Width (mm)	L_x (mm)	L_y (mm)	Cell angle (θ)
$l = h = 8.23$	$t=0.8$	$b=1$	293.93	195.1	30^0

Table 1: Geometric parameters of the unit cell and the whole lattice used for the finite element analysis.

multi-material lattices. These materials include tow versions of steel (ASTM-A36 and AISI 302), aluminium, bronze and brass. Elastic properties of these five materials are given in Table 2. These materials are selected for illustrative purposes only. The finale

No.	Material	Young's Modulus (GPa)	Poisson's ratio
1	Steel (ASTM-A36)	200	0.30
2	Steel (AISI 302)	180	0.30
3	Aluminium	70	0.33
4	Bronze	120	0.34
5	Brass	100	0.33

Table 2: Different materials and their elastic properties used in the finite element simulation.

element analysis methodology as well as the analytical expressions are not restricted to these materials.

Solid elements with 722019 nodes and 355208 elements are selected following a mesh convergence study for the finite element model. The validation is performed by considering

both single material and multimaterial case. The equivalent longitudinal Young's modulus is obtained considering the average displacements of all the nodes at the right edge of the lattice (distributed load application side). The strain is obtained by dividing this average displacement with the length of the lattice (L_x). The effective stress is derived by dividing the total force with the surface area of the edge. Finally, the equivalent Young's modulus is obtained by dividing the stress with the effective strain. Figure 5(b) shows a typical deformation pattern of the lattice material under the application of a uniformly distributed load at the right edge. In Table 3 analytical results are compared with finite element

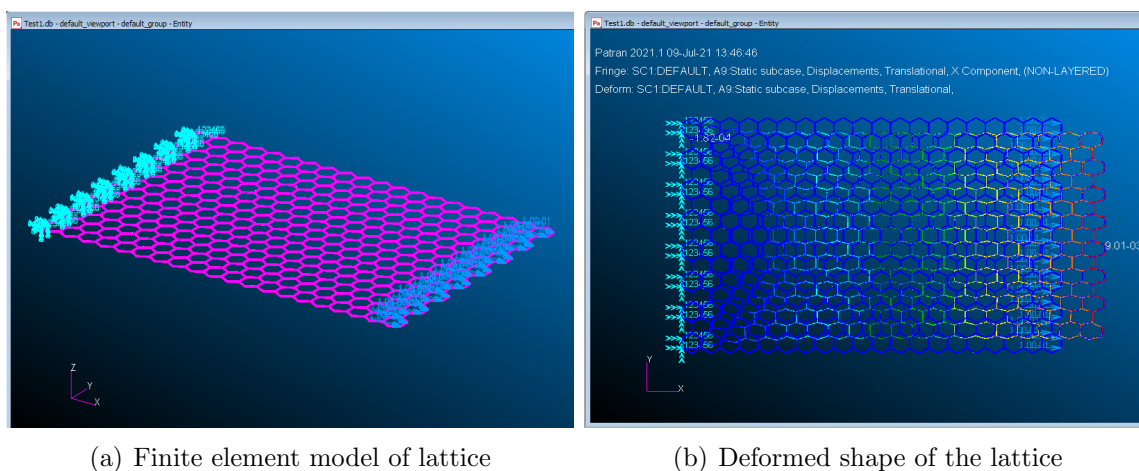


Fig. 5: Figure showing (a) Finite element model of the entire lattice. The left edge of the lattice is fixed and a uniformly distributed load is applied at the right edge for the analysis, (b) the deformed shape of the lattice for the application of load in the x direction.

simulation results. Equivalent normalised Young's modulus, i.e. $E_1/(E\alpha^3)$ is obtained for

Case	Materials	Analytical	FE	% error
1	Steel (ASTM-A36)	2.2458	2.2788	1.4692
2	Steel+AL	1.1645	1.2195	4.7295
3	Steel + Brass	1.4972	1.5829	5.7276
4	Steel+Bronze	1.6843	1.7632	4.6872
5	Steel(ASTM-A36+AISI 302)	2.1276	2.1695	1.9731
6	AL+Bronze	2.8367	2.8317	0.1758
7	AL+Brass	2.6421	2.6493	0.2725

Table 3: Comparison of the normalized longitudinal Young's modulus ($E_1/(E\alpha^3)$) for the hexagonal lattices obtained from closed form solution and finite element analysis. The normalization is carried out considering E value of Steel for the first 5 cases and for 6 and 7 the E value of Aluminium is considered.

both closed-form and FE based results. The value of $\alpha = t/l = 0.097$ and we considered Euler Bernoulli based closed-form expression for comparing with the FE results. For the multimaterial case, we consider $E_1 = E_3$ and various combinations of materials are used for numerical simulations. Results show that the finite element results differ from the closed-form solution though the error is within 6%.

6. The analysis of different material and geometric distributions

6.1. Effect of heterogeneity in material and geometric properties

In this section, the effect of multi-material and multi-thickness on the equivalent elastic properties are investigated for regular as well as auxetic lattices. Figures 6, 7 and 8 show the contour plots of normalized Young's moduli, Poisson's ratios and shear modulus respectively as a function of material disparity ratio and geometric disparity ratio considering both thin and thick beam assumption for regular hexagonal heterogeneous lattice. Whereas, figures 9, 10 and 11 represents the auxetic cases. We define the new measures, Material Disparity Ratio (MDR) and Geometric Disparity Ratio (GDR) as

$$\text{MDR} = \frac{E_2}{E_1} \quad \text{and} \quad \text{GDR} = \frac{\alpha_2}{\alpha_1} \quad (128)$$

We can observe from the figures that the values of Young's moduli and shear modulus monotonically increase with increasing MDR and GDR. For ν_{21} the value gradually decreases with an increase in MDR and GDR values. The trends of the contour lines for both thin and thick beam assumptions are the same whereas it is observed that the contour shift towards the right when the GDR increases. That means for constituent beams with thin beam assumption overestimates the values of the equivalent material properties for higher GDR values. The same is applicable to lower GDR values and it is clear from Fig. 8. The values of the equivalent material properties for conventional hexagonal lattice with cell angle 30° are shown by a black dot in each of these plots. These results show that for the equivalent elastic moduli, order-of-magnitude difference can be achieved by varying the MDR and GDR values. Therefore, it is clear from these contour plots that considering different material and thickness properties for the constituent beam members, the design space for the hexagonal lattice can be increased significantly.

6.2. Effect of material disparity

In this section, the effect of material disparity is investigated on the equivalent elastic properties of the hexagonal lattice. The thicknesses of all the constituent beam elements are the same but Young's modulus of the beam member b is varied. The Young's modulus of the vertical beam is kept the same as beam member a . The contour plots in this section represent the variation of equivalent elastic properties for regular as well as auxetic hexagonal lattice material. The contour plot, Fig. 12 of normalised elastic properties and Poisson's ratios are obtained considering the Euler Bernoulli model for constituent beams. The value of \bar{E}_1 decreases with increasing theta value and remain almost the same with increasing MDR. Whereas, \bar{E}_2 increase with theta and MDR ratio. For a particular value of theta the \bar{E}_1 increases up to MDR=2 after that the \bar{E}_1 value remain almost same with increasing MDR. Whereas, the value of \bar{E}_2 keep on increasing with increasing MDR value for a particular theta but the increase is gradual. The material disparity hardly affects ν_{12} and ν_{21} . The next contour plot Fig. 13 is the same investigation but considering Timoshenko beam theory for the constituent beam elements. Though there are differences in the values of the properties from the Euler Bernoulli case it is hard to recognize them from the plots. The trends are the same for all the properties. Figure 14 shows the variation of shear modulus with MD ratio and cell angle. It can be observed that for a particular value of MD ratio the value increases with cell angle. Though the trend for the regular and auxetic case are the same the increase in value for regular lattice

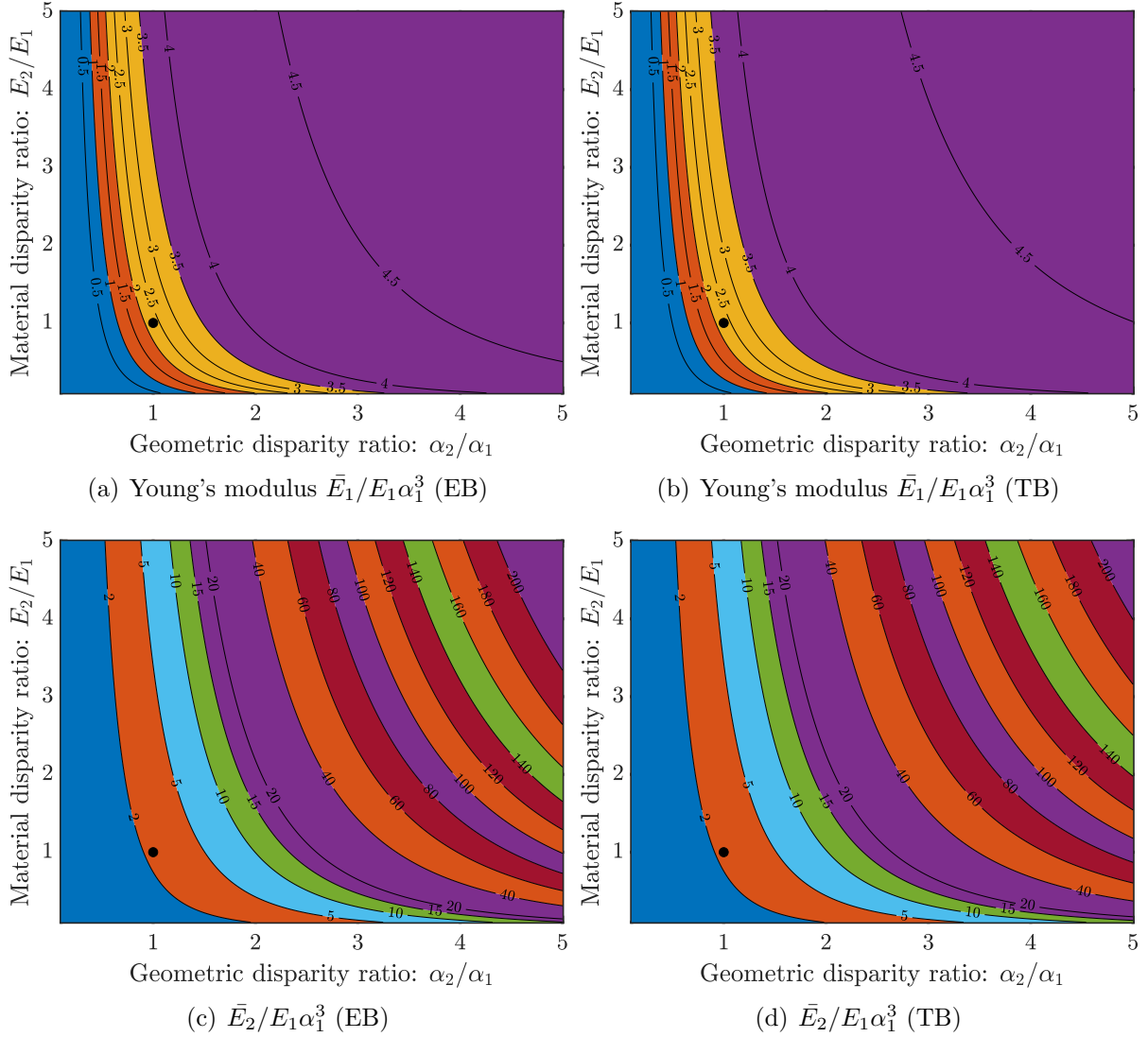


Fig. 6: Contour plot of the normalized equivalent elastic properties for hexagonal lattice as a function of the geometric and material disparity ratio. (a) \bar{E}_1 , Euler Bernoulli beam (EB) (b) \bar{E}_1 , Timoshenko beam (TB), (c) \bar{E}_2 , Euler Bernoulli beam (EB) and (d) \bar{E}_2 , Timoshenko beam (TB). The value of $\beta = 1$ and $\theta=30^\circ$. The value corresponding to the general isotropic case (GDR=1, MDR=1, $\theta=30^\circ$) is denoted by a black dot.

starts earlier. The values corresponding to the conventional regular hexagonal and auxetic lattice are shown in the plots as black dots and the plots reveal that the design space is enlarged due to the utilization of different constituent beam elements.

We can observe from the above sections that the effect of material and geometric variability on the equivalent elastic properties are different. The effect of geometric properties on the elastic properties is more significant considering the same disparity ratio. By changing the geometric disparity ratio the values of the elastic constants can be increased significantly. Whereas, the material variability can be utilized where we need a very much controlled increase.

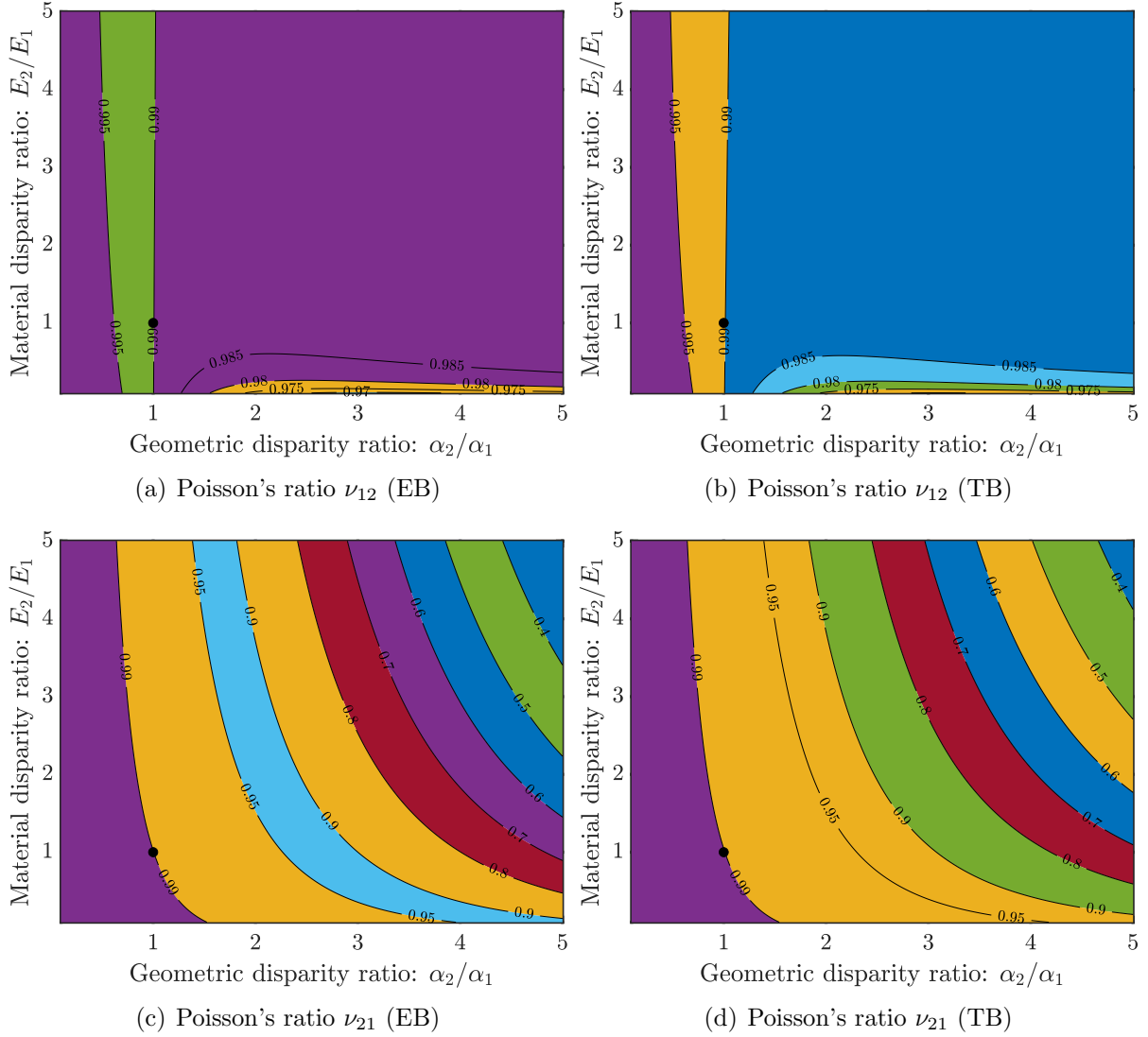


Fig. 7: Contour plot of the Poisson's ratio for hexagonal lattice as a function of the geometric and material disparity ratio. (a) ν_{12} , Euler Bernoulli beam (EB) (b) ν_{12} , Timoshenko beam (TB), (c) ν_{21} , Euler Bernoulli beam (EB) and (d) ν_{21} , Timoshenko beam (TB). The value of $\beta = 1$ and $\theta = 30^\circ$. The value corresponding to the general isotropic case (GDR=1, MDR=1, $\theta = 30^\circ$) is denoted by a black dot.

6.3. Effect of geometric disparity

This section deals with the effect of geometric disparity on the equivalent elastic moduli of the hexagonal lattice (both regular and auxetic). Here, we consider that the material of all the constituent beam elements is the same but the thickness of the two slant beam members are varying. The thickness of the vertical beam is kept the same as beam member a and the thickness of the beam member b is kept on increasing to obtain the contour plots. Figure 15 shows the contour plot of the normalised elastic properties and Poisson's ratios considering the Euler Bernoulli model for constituent beams. It can be observed that the \bar{E}_1 decreases with increasing theta value and for all values of GDR. Whereas, \bar{E}_2 increase with theta and GDR. For a particular value of theta the \bar{E}_1 increases up to $\alpha_2/\alpha_1 = 2$ after that the \bar{E}_1 value remain almost same with increasing GDR. Whereas, the value of \bar{E}_2 keep on increasing with increasing GDR value for a particular theta and

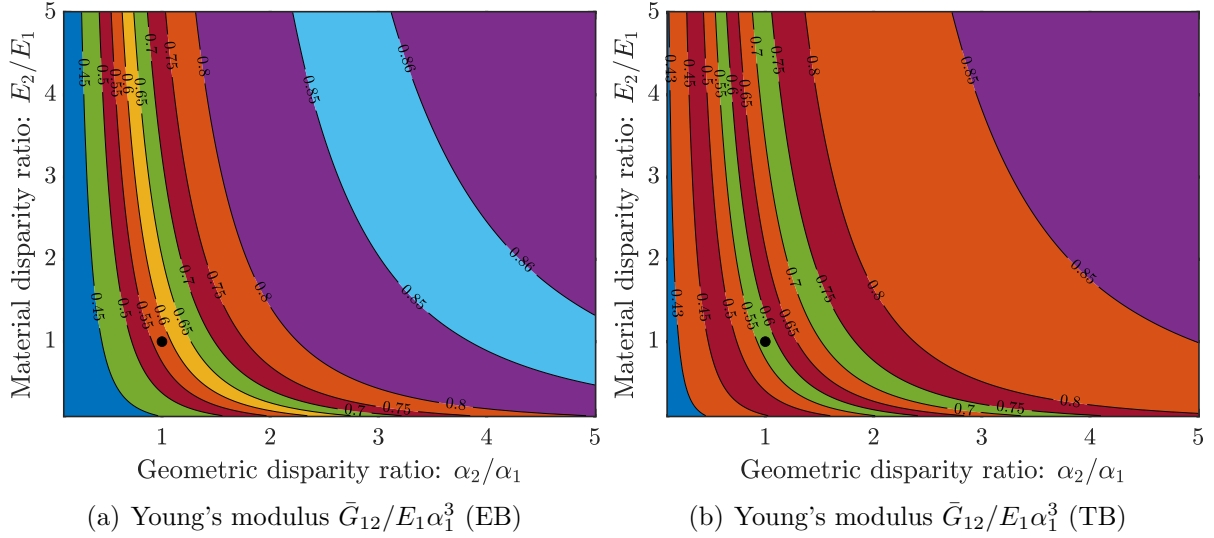


Fig. 8: Contour plot of the normalized equivalent shear modulus for hexagonal lattice as a function of the geometric and material disparity ratio. (a) \bar{G}_{12} , Euler Bernoulli beam (EB) (b) \bar{G}_{12} , Timoshenko beam (TB). The value of $\beta = 1$ and $\theta=30^\circ$. The value corresponding to the general isotropic case (GDR=1, MDR=1, $\theta=30^\circ$) is denoted by a black dot.

the increase is very fast. The value of ν_{12} remains almost the same with increasing GDR value and it decreases with increasing theta. The trend of ν_{21} is increasing for higher theta values and it decreases with GDR value for a particular theta. The value of G_{12} increases with theta and also with GDR value but at a slow rate after GDR value 2. The next contour plot Fig. 16 is the same investigation but considering Timoshenko beam theory for the constituent beam elements. Figure 14 shows the variation of shear modulus with MD ratio and cell angle.

7. Conclusions

The most general form of 2D heterogeneous hexagonal lattices was proposed in this paper through the combination of multi-material and multi-thickness elements. A physics-based analytical prediction approach for the equivalent elastic properties of such heterogeneous hexagonal lattices was developed. The equivalent elastic properties consist of five quantities, namely, the Young's moduli and Poisson's ratios in both directions and the shear modulus. The analytical formulation was based on a unit cell comprised of three different beams with different thicknesses and material properties. A novel aspect of the theoretical derivations is the employment of physics-based compatibility conditions and boundary conditions. The mechanical analysis was implemented in such a way that the equivalent elastic properties are expressed in terms of the elements of the stiffness matrices of the constituent beams. This allowed the genetic expressions to be applied for special cases of thin and thick-walled lattices using Euler-Bernoulli and Timoshenko beam theories, respectively. The closed-form expressions of the equivalent elastic properties were obtained in terms of the geometric properties of the hexagonal unit cell and material properties and thicknesses of the cell walls. A rigorous finite element validation was performed for the closed-form expressions using the commercial software NASTRAN.

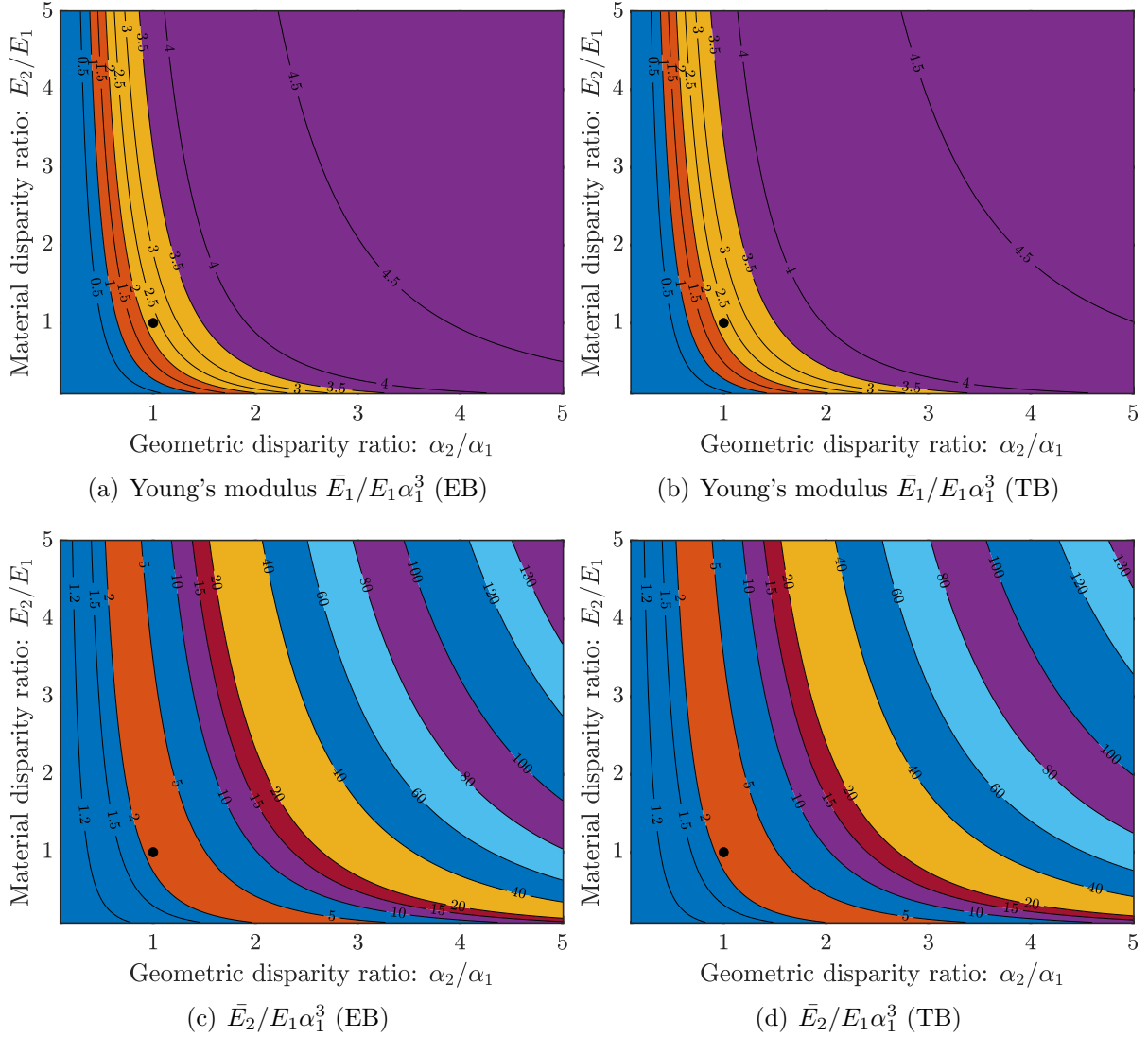


Fig. 9: Contour plot of the normalized equivalent elastic properties for auxetic hexagonal lattice as a function of the geometric and material disparity ratio. (a) \bar{E}_1 , Euler Bernoulli beam (EB) (b) \bar{E}_1 , Timoshenko beam (TB), (c) \bar{E}_2 , Euler Bernoulli beam (EB) and (d) \bar{E}_2 , Timoshenko beam (TB). The value of $\beta = 2$ and $\theta = -30^\circ$. The value corresponding to the regular lattice (GDR=1, MDR=1, $\theta=30^\circ$) is denoted by a black dot.

Validation results demonstrate excellent accuracy (less than 6% error) of the new expressions derived in the paper. Variations in the material and geometric properties of the cell walls are quantified by defining the Material Disparity Ratio (MDR) and the Geometric Disparity Ratio (GDR). Numerical results obtained show that for certain combinations of MDR and GDR, the equivalent elastic moduli of a heterogeneous lattice can be orders-of-magnitude different from its homogeneous counterpart.

The novelty of this work lies in the conceptual development of heterogeneous lattices and subsequently the generalised analytical formulation to quantify the equivalent elastic properties. The key features of this present work include:

- A general methodology to derive the equivalent elastic properties of heterogeneous hexagonal lattice considering the coefficients of the stiffness matrix of constituent

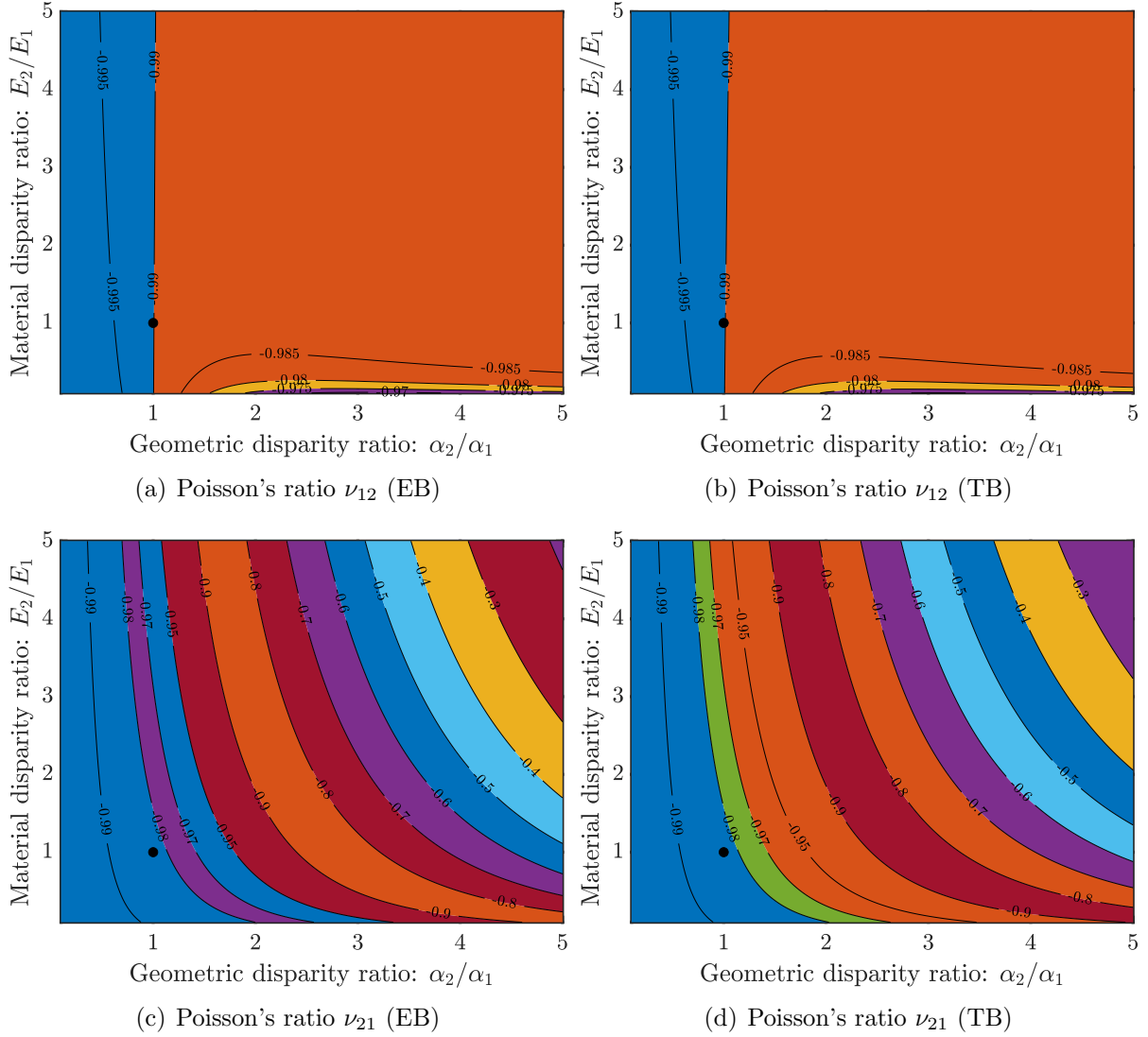


Fig. 10: Contour plot of the Poisson's ratio for auxetic hexagonal lattice as a function of the geometric and material disparity ratio. (a) ν_{12} , Euler Bernoulli beam (EB) (b) ν_{12} , Timoshenko beam (TB), (c) ν_{21} , Euler Bernoulli beam (EB) and (d) ν_{21} , Timoshenko beam (TB). The value of $\beta = 2$ and $\theta = -30^\circ$. The value corresponding to the regular lattice (GDR=1, MDR=1, $\theta=30^\circ$) is denoted by a black dot.

beams.

- The most general analytical expressions for equivalent elastic properties of 2D heterogeneous hexagonal lattices from which other geometries and special cases can be derived in a straightforward manner.
- Investigation of thin-walled and thick-walled lattices and closed-form expressions of some physically relevant limiting cases.
- The framework of an enriched design space for lattice materials due to the generalisation of the constituent beam elements from a geometric and material perspective.

The closed-form expressions can be utilised as a benchmark solution for further studies. The formulation can be utilised or extended for a large class of constituent beam

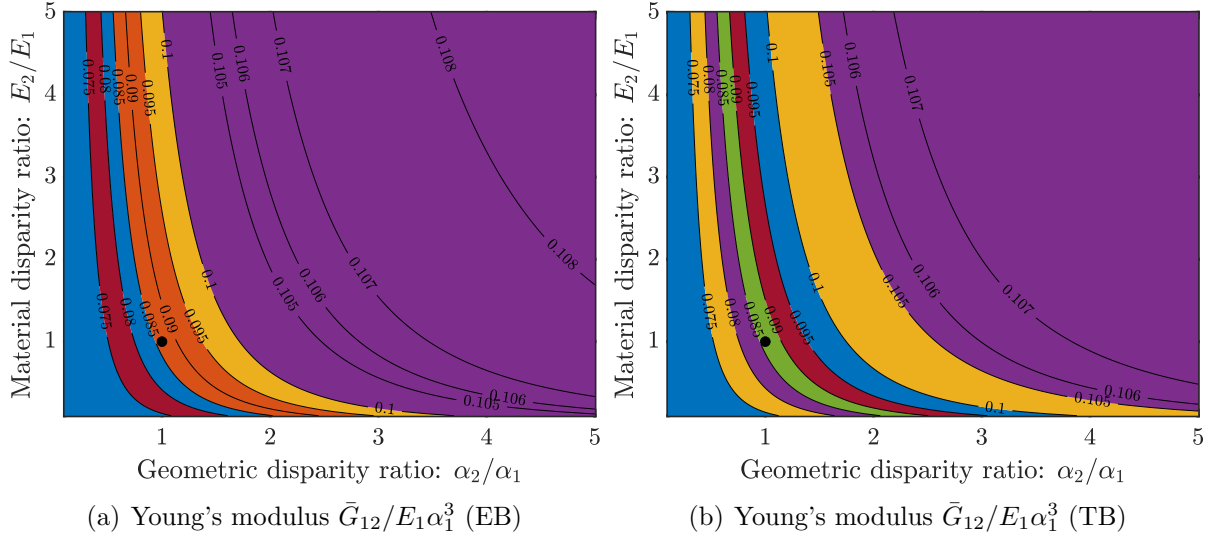


Fig. 11: Contour plot of the normalized equivalent shear modulus for auxetic hexagonal lattice as a function of the geometric and material disparity ratio. (a) \bar{G}_{12} , Euler Bernoulli beam (EB) (b) \bar{G}_{12} , Timoshenko beam (TB). The value of $\beta = 2$ and $\theta = -30^\circ$. The value corresponding to the regular lattice (GDR=1, MDR=1, $\theta=30^\circ$) is denoted by a black dot.

elements such as beam with varying depth and functionally graded beams as the expressions are in terms of the elements of the stiffness matrix. The analytical expressions are well suited for the design of heterogeneous lattices with highly tailored effective elastic properties as constraints. Future works arising from this paper will include buckling and instability analysis, dynamic behaviour such as bandgap studies and nonlinear analysis of heterogeneous lattices.

References

- [1] T. Frenzel, M. Kadic, M. Wegener, Three-dimensional mechanical metamaterials with a twist, *Science* 358 (6366) (2017) 1072–1074.
- [2] L. Gibson, M. F. Ashby, *Cellular Solids Structure and Properties*, Cambridge University Press, Cambridge, UK, 1999.
- [3] N. A. Fleck, V. S. Deshpande, M. F. Ashby, Micro-architected materials: past, present and future, *Proceedings of the Royal Society A: Mathematical, Physical and Engineering Sciences* 466 (2121) (2010) 2495–2516.
- [4] S. A. Cummer, J. Christensen, A. Alù, Controlling sound with acoustic metamaterials, *Nature Reviews Materials* 1 (3) (2016) 1–13.
- [5] G. Hunt, T. Dodwell, Complexity in phase transforming pin-jointed auxetic lattices, *Proceedings of the Royal Society A* 475 (2224) (2019) 20180720.
- [6] H. Wang, D. Zhao, Y. Jin, M. Wang, T. Mukhopadhyay, Z. You, Modulation of multi-directional auxeticity in hybrid origami metamaterials, *Applied Materials Today* 20 (2020) 100715.
- [7] H. Xu, D. Pasini, Structurally efficient three-dimensional metamaterials with controllable thermal expansion, *Scientific reports* 6 (1) (2016) 1–8.
- [8] T. Li, X. Hu, Y. Chen, L. Wang, Harnessing out-of-plane deformation to design 3d architected lattice metamaterials with tunable poisson's ratio, *Scientific reports* 7 (1) (2017) 1–10.
- [9] Z. Jia, F. Liu, X. Jiang, L. Wang, Engineering lattice metamaterials for extreme property, programmability, and multifunctionality, *Journal of Applied Physics* 127 (15) (2020) 150901.
- [10] A. Bacigalupo, M. Lepidi, G. Gnecco, F. Vadalà, L. Gambarotta, Optimal design of the band structure for beam lattice metamaterials, *Frontiers in Materials* 6 (2019) 2.

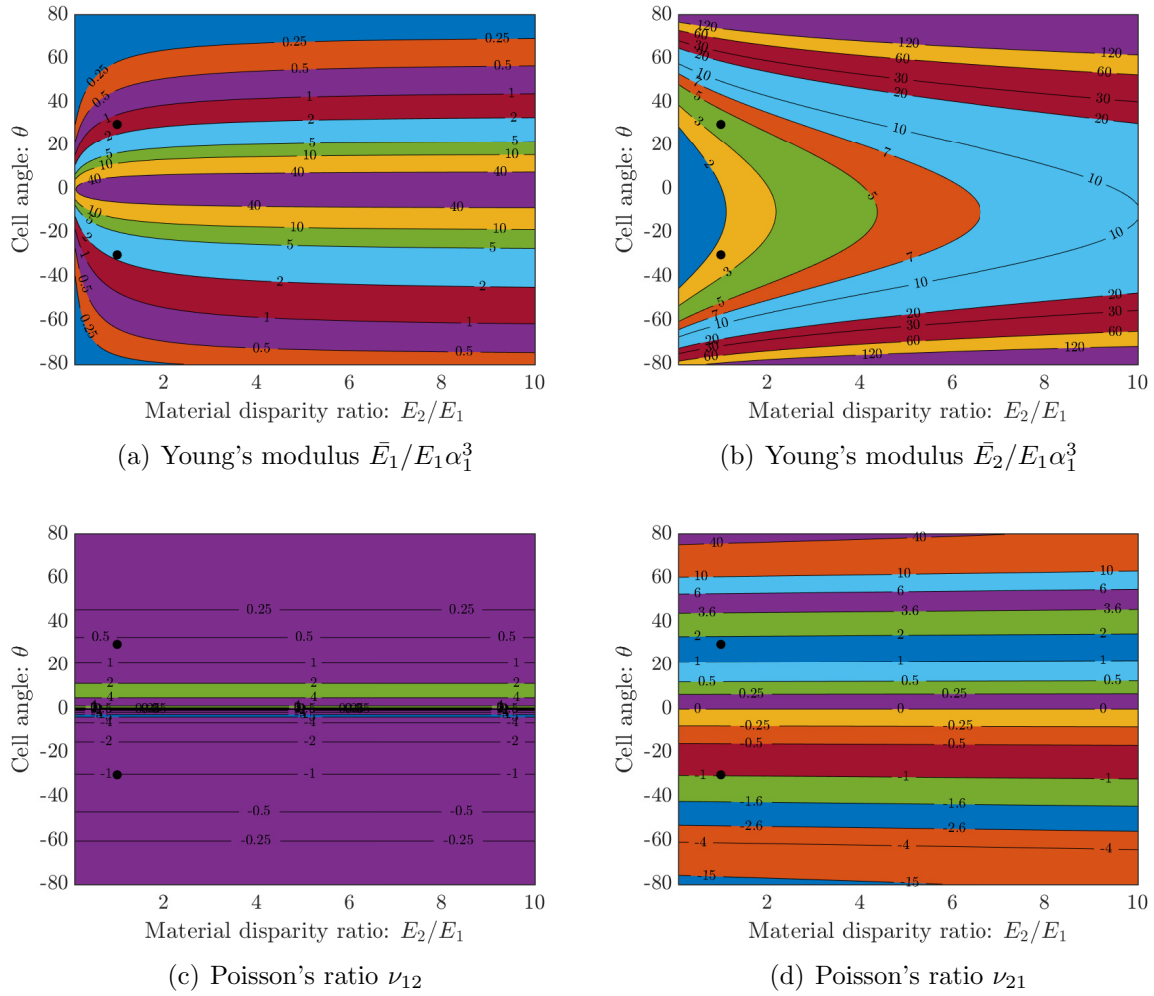


Fig. 12: Contour plot of the normalized equivalent elastic moduli and Poisson's ratios as a function of the cell angle (θ) and material disparity ratio (MDR= E_2/E_1) considering thin beam assumption. The value of $\alpha_1 = 0.05$, $\beta = 2$ and $E_1=70$ Gpa. The values corresponding to the regular lattice (MDR=1, $\theta = \pm 30^\circ$) are denoted by black dots.

- [11] S. Balawi, J. Abot, A refined model for the effective in-plane elastic moduli of hexagonal honeycombs, *Composite Structures* 84 (2) (2008) 147–158.
- [12] B. Niu, B. Wang, Directional mechanical properties and wave propagation directionality of kagome honeycomb structures, *European Journal of Mechanics-A/Solids* 57 (2016) 45–58.
- [13] S. Adhikari, The in-plane mechanical properties of highly compressible and stretchable 2d lattices, *Composite Structures* 272 (2021) 114167.
- [14] A. Karakoç, K. Santaoja, J. Freund, Simulation experiments on the effective in-plane compliance of the honeycomb materials, *Composite Structures* 96 (2013) 312–320.
- [15] T. Baran, M. Öztürk, In-plane elasticity of a strengthened re-entrant honeycomb cell, *European Journal of Mechanics-A/Solids* 83 (2020) 104037.
- [16] Q. Chen, N. M. Pugno, In-plane elastic buckling of hierarchical honeycomb materials, *European Journal of Mechanics-A/Solids* 34 (2012) 120–129.
- [17] S. Adhikari, The eigenbuckling analysis of hexagonal lattices: Closed-form solutions, *Proceedings of the Royal Society of London, Series - A* 477 (2251) (2021) 20210244.
- [18] V. E. Gasparetto, M. S. ElSayed, Shape transformers for phononic band gaps tuning in two-dimensional bloch-periodic lattice structures, *European Journal of Mechanics-A/Solids* (2021) 104278.

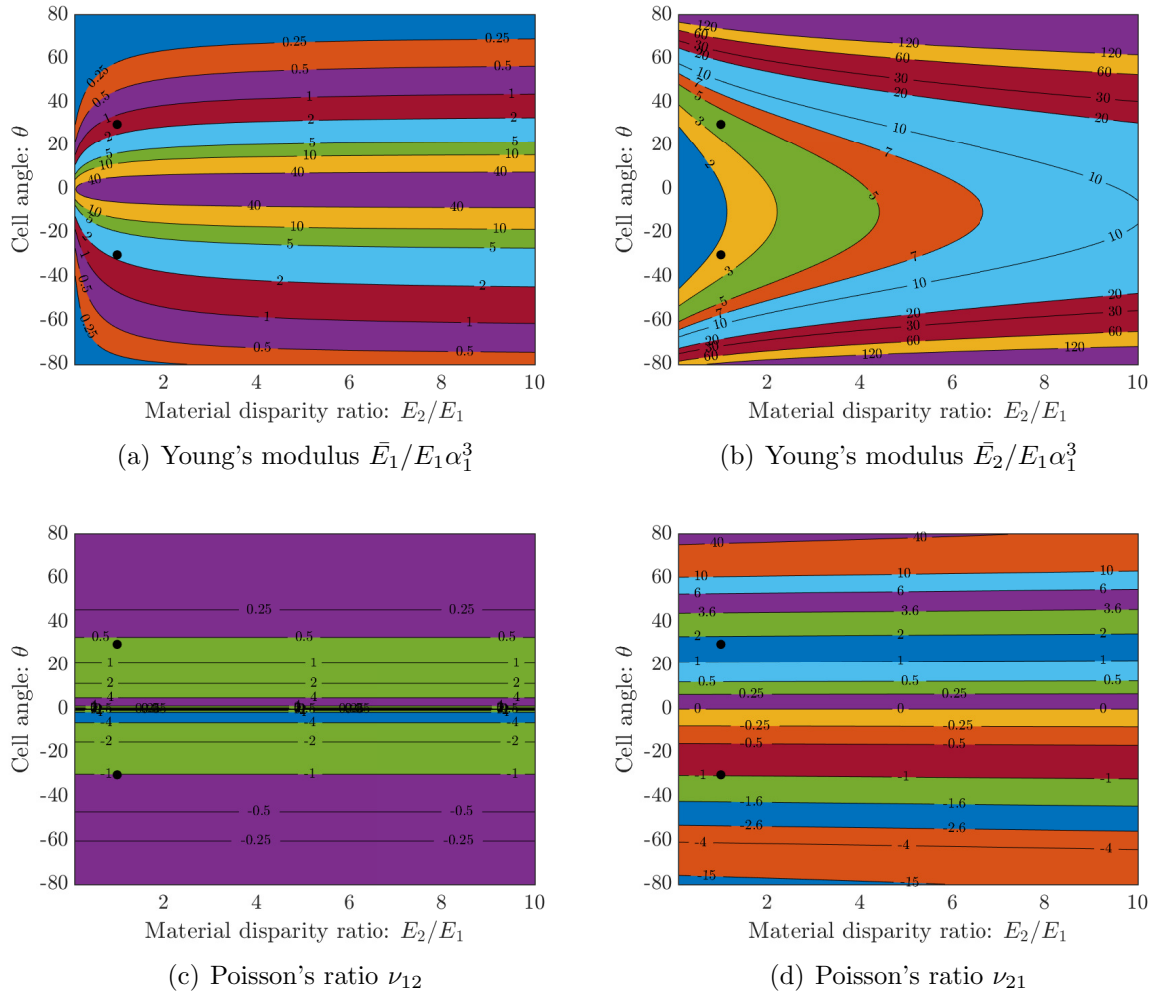


Fig. 13: Contour plot of the normalized equivalent elastic moduli and Poisson's ratio as a function of the cell angle (θ) and material disparity ratio (MDR= E_2/E_1) considering thick beam assumption. The value of $\alpha_1 = 0.05$, $\beta = 2$ and $E_1=70$ Gpa. The values corresponding to the regular lattice (MDR=1, $\theta = \pm 30^\circ$) are denoted by black dots.

- [19] L. Gibson, K. Easterling, M. F. Ashby, The structure and mechanics of cork, Proceedings of the Royal Society of London. A. Mathematical and Physical Sciences 377 (1769) (1981) 99–117.
- [20] M. S. Rad, Y. Prawoto, Z. Ahmad, Analytical solution and finite element approach to the 3d re-entrant structures of auxetic materials, Mechanics of Materials 74 (2014) 76–87.
- [21] T. Mukhopadhyay, S. Adhikari, Effective in-plane elastic moduli of quasi-random spatially irregular hexagonal lattices, International Journal of Engineering Science 119 (2017) 142–179.
- [22] Y. Chen, H. Hu, In-plane elasticity of regular hexagonal honeycombs with three different joints: A comparative study, Mechanics of Materials 148 (2020) 103496.
- [23] S. Adhikari, T. Mukhopadhyay, X. Liu, Broadband dynamic elastic moduli of honeycomb lattice materials: A generalized analytical approach, Mechanics of Materials (2021) 103796.
- [24] I. G. Masters, K. E. Evans, Models for the elastic deformation of honeycombs, Composite Structures 35 (4) (1996) 403–422.
- [25] F. Abd El-Sayed, R. Jones, I. Burgess, A theoretical approach to the deformation of honeycomb based composite materials, Composites 10 (4) (1979) 209–214.
- [26] C. Zschernack, M. A. Wadee, C. Völlmecke, Nonlinear buckling of fibre-reinforced unit cells of lattice materials, Composite Structures 136 (2016) 217–228.
- [27] T. Huang, Y. Gong, S. Zhao, Effective in-plane elastic modulus of a periodic regular hexagonal

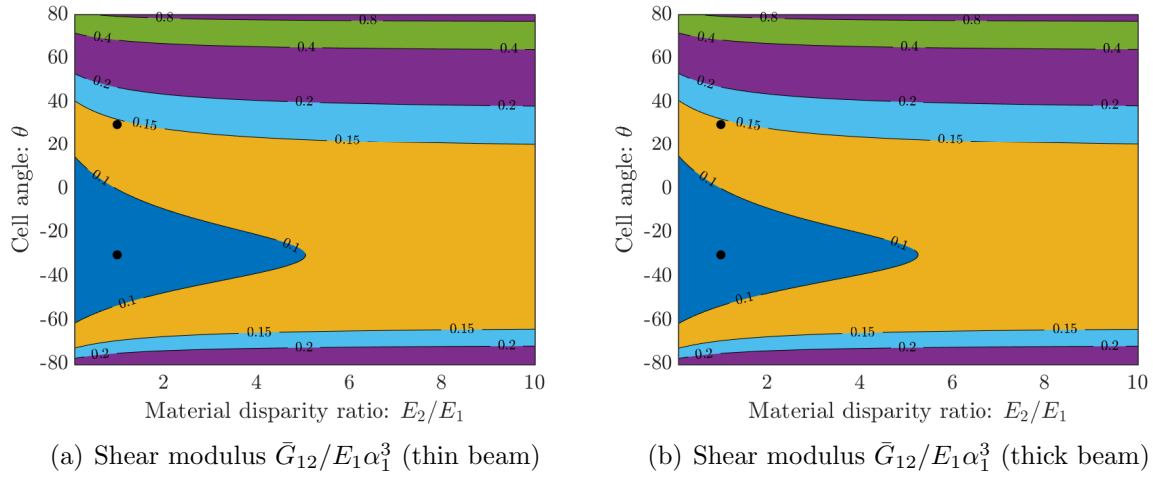
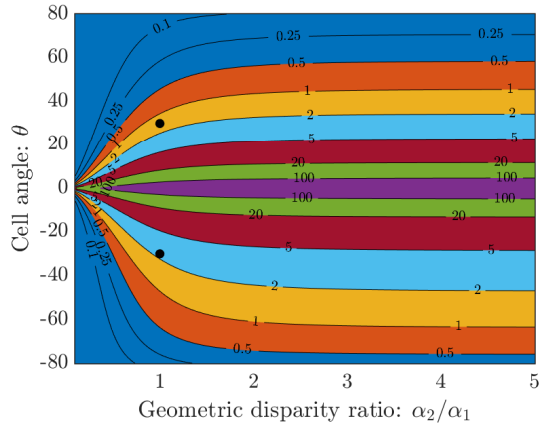
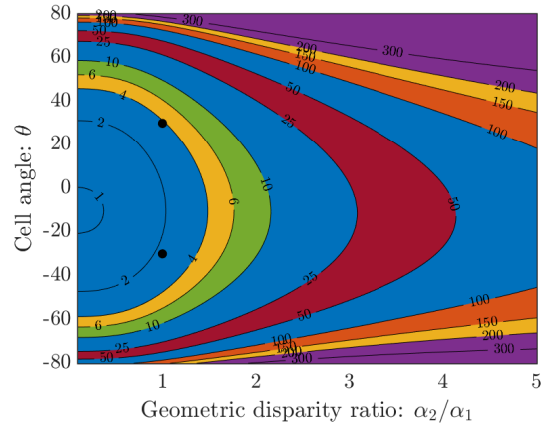


Fig. 14: Contour plot of the normalized equivalent shear modulus as a function of the cell angle (θ) and material disparity ratio (MDR= E_2/E_1) considering (a) thin and (b) thick beam assumption. The value of $\alpha_1 = 0.05$, $\beta = 2$ and $E_1 = 70$ Gpa. The values corresponding to the regular lattice (MDR=1, $\theta = \pm 30^\circ$) are denoted by black dots.

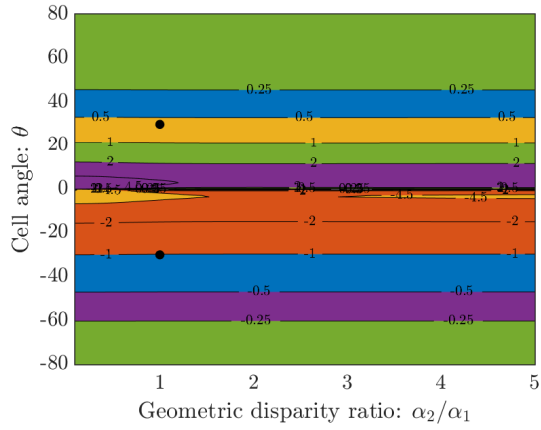
- honeycomb core with thick walls, *Journal of Engineering Mechanics* 144 (2) (2018) 06017019.
- [28] S. Balawi, J. Abot, The effect of honeycomb relative density on its effective in-plane elastic moduli: An experimental study, *Composite Structures* 84 (4) (2008) 293–299.
- [29] F. Ongaro, Estimation of the effective properties of two-dimensional cellular materials: a review, *Theoretical and Applied Mechanics Letters* 8 (4) (2018) 209–230.
- [30] M. S. Hefzy, A. H. Nayfeh, Shear deformation plate continua of large double layered space structures, *International journal of solids and structures* 22 (12) (1986) 1455–1469.
- [31] D. Chen, X. Zheng, Multi-material additive manufacturing of metamaterials with giant, tailorable negative poisson's ratios, *Scientific reports* 8 (1) (2018) 1–8.
- [32] A. Bandyopadhyay, B. Heer, Additive manufacturing of multi-material structures, *Materials Science and Engineering: R: Reports* 129 (2018) 1–16.
- [33] S. Tibbits, 4d printing: multi-material shape change, *Architectural Design* 84 (1) (2014) 116–121.
- [34] D. Kang, S. Park, Y. Son, S. Yeon, S. H. Kim, I. Kim, Multi-lattice inner structures for high-strength and light-weight in metal selective laser melting process, *Materials & Design* 175 (2019) 107786.
- [35] P. Vogiatzis, S. Chen, X. Wang, T. Li, L. Wang, Topology optimization of multi-material negative poisson's ratio metamaterials using a reconciled level set method, *Computer-Aided Design* 83 (2017) 15–32.
- [36] T. Mukhopadhyay, S. Naskar, S. Adhikari, Anisotropy tailoring in geometrically isotropic multi-material lattices, *Extreme Mechanics Letters* 40 (2020) 100934.
- [37] D. Dawe, *Matrix and Finite Element Displacement Analysis of Structures*, Oxford University Press, Oxford, UK, 1984.
- [38] M. Petyt, *Introduction to Finite Element Vibration Analysis*, Cambridge University Press, Cambridge, UK, 1990.
- [39] E. Nolde, A. Pichugin, J. Kaplunov, An asymptotic higher-order theory for rectangular beams, *Proceedings of the Royal Society A: Mathematical, Physical and Engineering Sciences* 474 (2214) (2018) 20180001.
- [40] S. Malek, L. Gibson, Effective elastic properties of periodic hexagonal honeycombs, *Mechanics of Materials* 91 (2015) 226–240.



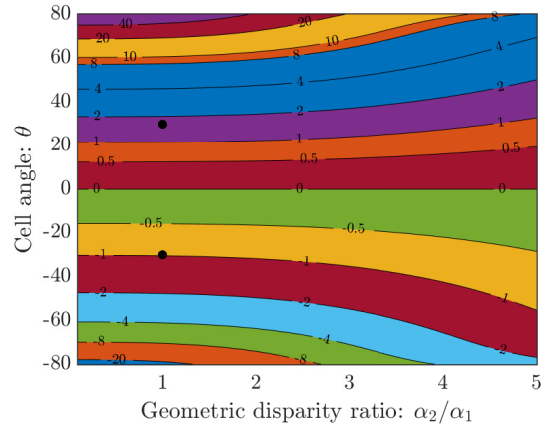
(a) Young's modulus $\bar{E}_1/E_1\alpha_1^3$



(b) Young's modulus $\bar{E}_2/E_1\alpha_1^3$

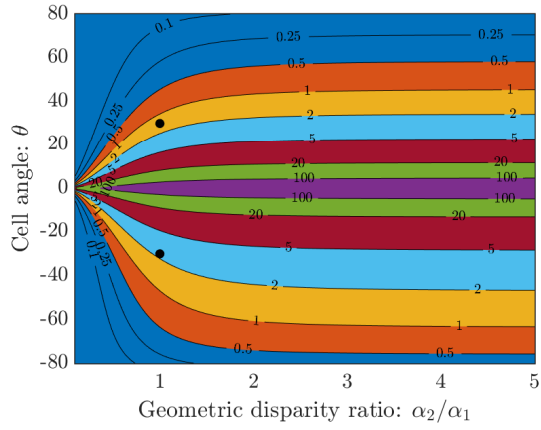


(c) Poisson's ratio ν_{12}

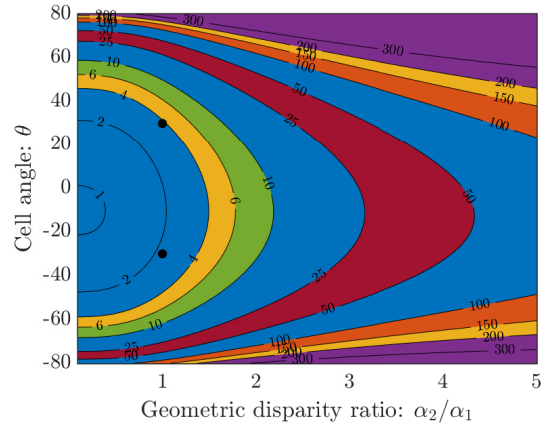


(d) Poisson's ratio ν_{21}

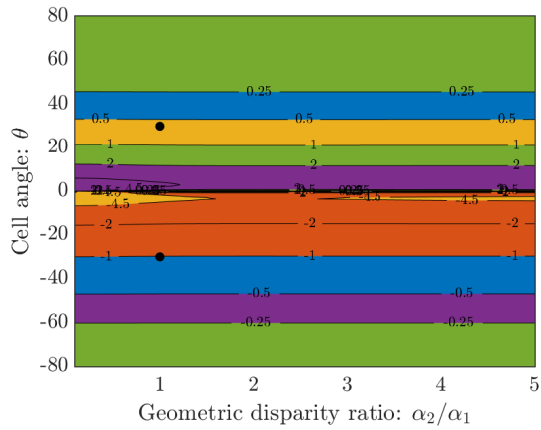
Fig. 15: Contour plot of the normalized equivalent elastic moduli and Poisson's ratio as a function of the cell angle (θ) and geometric disparity ratio (GDR= α_2/α_1) considering thin beam assumption. The value of $\alpha_1 = 0.05$, $\beta = 2$ and $E_1=70$ Gpa. The values corresponding to the regular lattice (GDR=1, $\theta = \pm 30^\circ$) are denoted by black dots.



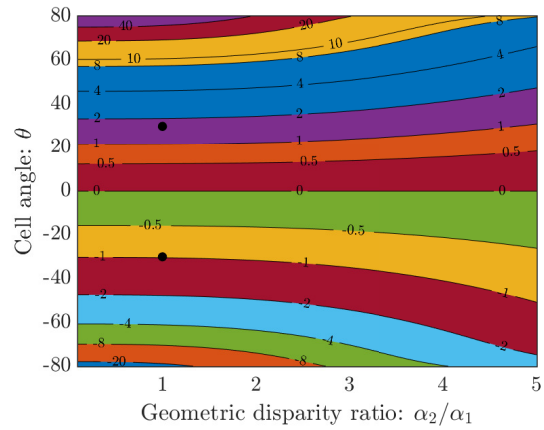
(a) Young's modulus $\bar{E}_1/E_1\alpha_1^3$



(b) Young's modulus $\bar{E}_2/E_1\alpha_1^3$

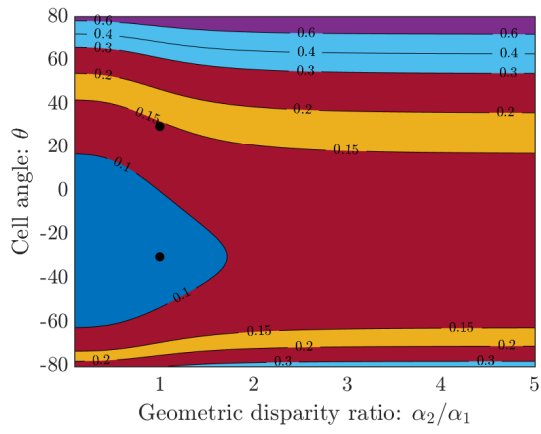


(c) Poisson's ratio ν_{12}

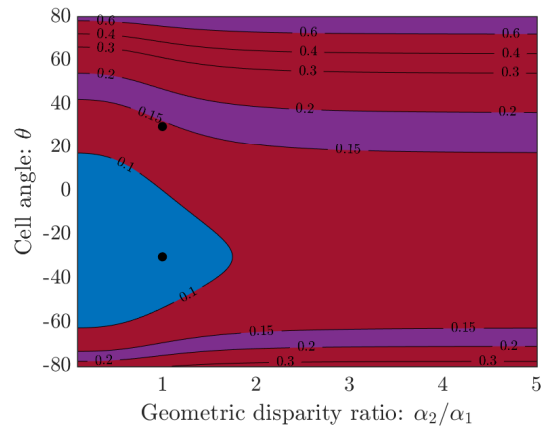


(d) Poisson's ratio ν_{21}

Fig. 16: Contour plot of the normalized equivalent elastic modulli and Poisson's ratio as a function of the cell angle (θ) and geometric disparity ratio ($GDR=\alpha_2/\alpha_1$) considering thick beam assumption. The value of $\alpha_1 = 0.05$, $\beta = 2$ and $E_1=70$ Gpa. The values corresponding to the regular lattice ($GDR=1$, $\theta = \pm 30^\circ$) are denoted by black dots.



(a) Shear modulus $\bar{G}_{12}/E_1\alpha_1^3$ (thin beam)



(b) Shear modulus $\bar{G}_{12}/E_1\alpha_1^3$ (thick beam)

Fig. 17: Contour plot of the normalized equivalent shear modulus as a function of the cell angle (θ) and geometric disparity ratio ($\text{GDR}=\alpha_2/\alpha_1$) considering (a) thin and (b) thick beam assumption. The values corresponding to the regular lattice ($\text{GDR}=1, \theta = \pm 30^\circ$) are denoted by black dots.